Contrib Mineral Petrol (2002) 143: 416–437
DOI 10.1007/s00410-002-0354-9

O. Tapani Rämö · James P. Calzia · Paula J. Kosunen

Geochemistry of Mesozoic plutons, southern Death Valley region, California: Insights into the origin of Cordilleran interior magmatism

Received: 5 June 2000 / Accepted: 20 January 2002 / Published online: 26 April 2002

Abstract Mesozoic granitoid plutons in the southern Death Valley region of southeastern California reveal substantial compositional and isotopic diversity for Mesozoic magmatism in the southwestern US Cordillera. Jurassic plutons of the region are mainly calc-alkaline mafic granodiorites with ϵ_{Ndi} of –5 to –16, $^{87}Sr/^{86}Sr_i$ of 0.707–0.726, and $^{206}Pb/^{204}Pb_i$ of 17.5–20.0. Cretaceous granitoids of the region are mainly monzogranites with ϵ_{Ndi} of –6 to –19, $^{87}Sr/^{86}Sr_i$ of 0.707–0.723, and $^{206}Pb/^{204}Pb_i$ of 17.4–18.6. The granitoids were generated by mixing of mantle-derived mafic melts and pre-existing crust – some of the Cretaceous plutons represent melting of Paleoproterozoic crust that, in the southern Death Valley region, is exceptionally heterogeneous. A Cretaceous gabbro on the southern flank of the region has an unusually juvenile composition (ϵ_{Ndi} –3.2, $^{87}Sr/^{86}Sr_i$ 0.7060). Geographic position of the Mesozoic plutons and comparison with Cordilleran plutonism in the Mojave Desert show that the Precambrian lithosphere (craton margin) in the eastern Mojave Desert region may consists of two crustal blocks separated by a more juvenile terrane.

Introduction

Mesozoic plutonism in the Mojave Desert of southern California has been studied in considerable detail during the last decade (e.g., Fox and Miller 1990; John and Wooden 1990; Miller et al. 1990; Young et al. 1992; Karlstrom et al. 1993; Miller and Wooden 1994; Allen et al. 1995; Barth et al. 1995; Gerber et al. 1995; Miller and Glazner 1995). These studies rely on geochemical and isotopic data from Jurassic and Cretaceous plutons for petrogenetic models regarding the origin of the magmas and the composition of their source rocks. Data on Jurassic plutons, for instance, have revealed differences between lithospheric domains in the central (Miller and Glazner 1995; Miller et al. 1995) and eastern (Young et al. 1992; Gerber et al. 1995) Mojave Desert, with the former showing a more juvenile character (higher initial ϵ_{Nd} and lower initial $^{87}Sr/^{86}Sr$). Cretaceous plutons, on the other hand, are more heterogeneous (Allen et al. 1995) and tend to have had a larger component of pre-existing (Precambrian) crust in their source rocks (e.g., John and Wooden 1990; Miller et al. 1990; Hanchar et al. 1994; Miller and Wooden 1994).

In this paper, we present new petrologic, chemical, and isotopic data for Jurassic and Cretaceous plutons in the southern Death Valley region of southeastern California. We show that the Jurassic and Cretaceous granitoid rocks are chemically and isotopically different from Mesozoic plutonic rocks in the central and eastern Mojave Desert. We also describe the chemical and isotopic character of Jurassic and Cretaceous mafic rocks associated with the granitoid plutons. These data are combined into models on the origin of Mesozoic plutons in the southern Death Valley region. Overall, our data suggest that distinct lithospheric domains existed in the Mojave Desert during the Mesozoic and that the southern Death Valley region hosts a crustal segment with an anomalously juvenile character.

Geologic setting

The southern Death Valley region (Calzia and Rämö 2000) covers approximately 15,000 km^2 on the eastern flank of Jurassic and Cretaceous magmatic arcs in

O.T. Rämö (✉)
Department of Geology, P.O. Box 64,
00014 University of Helsinki, Finland
E-mail: tapani.ramo@helsinki.fi
Tel.: +358-40-5260636
Fax: +358-9-19150826

J.P. Calzia
US Geological Survey, 345 Middlefield Rd.,
Menlo Park, California 94025, USA

P.J. Kosunen
Department of Geology, P.O. Box 64,
00014 University of Helsinki, Finland

Editorial responsibility: I.S.E. Carmichael

southeastern California (Fig. 1). The oldest rocks in this region are Paleoproterozoic (>1,700 Ma) gneisses, schists, and migmatites intruded by ~1,700, 1,660, and 1,400 Ma granitoids (Wooden and Miller 1990). These cratonic rocks are unconformably overlain by approximately 2,100 m of conglomerate, sandstone, shale, and carbonate rocks of the Mesoproterozoic Pahrump Group (Calzia 1990). The Pahrump Group is intruded by 1,100 Ma (Heaman and Grotzinger 1992) diabase dikes and sills (Wright 1967), and is overlain by 3,000–5,000 m of Neoproterozoic to Triassic clastic and carbonate rocks of the Cordilleran geocline. The Proterozoic to Mesozoic rocks are intruded by Mesozoic plutons ranging in composition from granite to gabbro and by Tertiary (mainly middle Miocene) granites (Calzia 1990). All of these rocks are unconformably overlain by late Tertiary sedimentary and volcanic rocks and Quaternary alluvial deposits.

Fig. 1. Geological map of the southern Death Valley region. Sample locations and ϵ_{Ndi} values of the Mesozoic plutons are indicated. The Late Cretaceous Hall Canyon pluton (Mahood et al. 1996) is located approximately 20 km south of sample 123/95 in the northwestern part of the region. *Inset* shows area relative to southern California and position of Jurassic and Cretaceous magmatic arcs (Fox and Miller 1990). Modified from Rämö and Calzia (1998) and Beckerman et al. (1982)

Petrography

We collected 19 samples of Mesozoic plutons within the southern Death Valley region for geochemical analysis. The sampling sites were chosen to obtain representative samples of each pluton and to achieve good areal, temporal, and petrographic coverage of the plutons. Sampled locations are shown in Fig. 1, modal compositions of the samples are listed in Table 1 and shown in Fig. 2, and petrographic descriptions are given in the Appendix.

Jurassic plutons are less abundant than Cretaceous plutons and are found as relatively small bodies

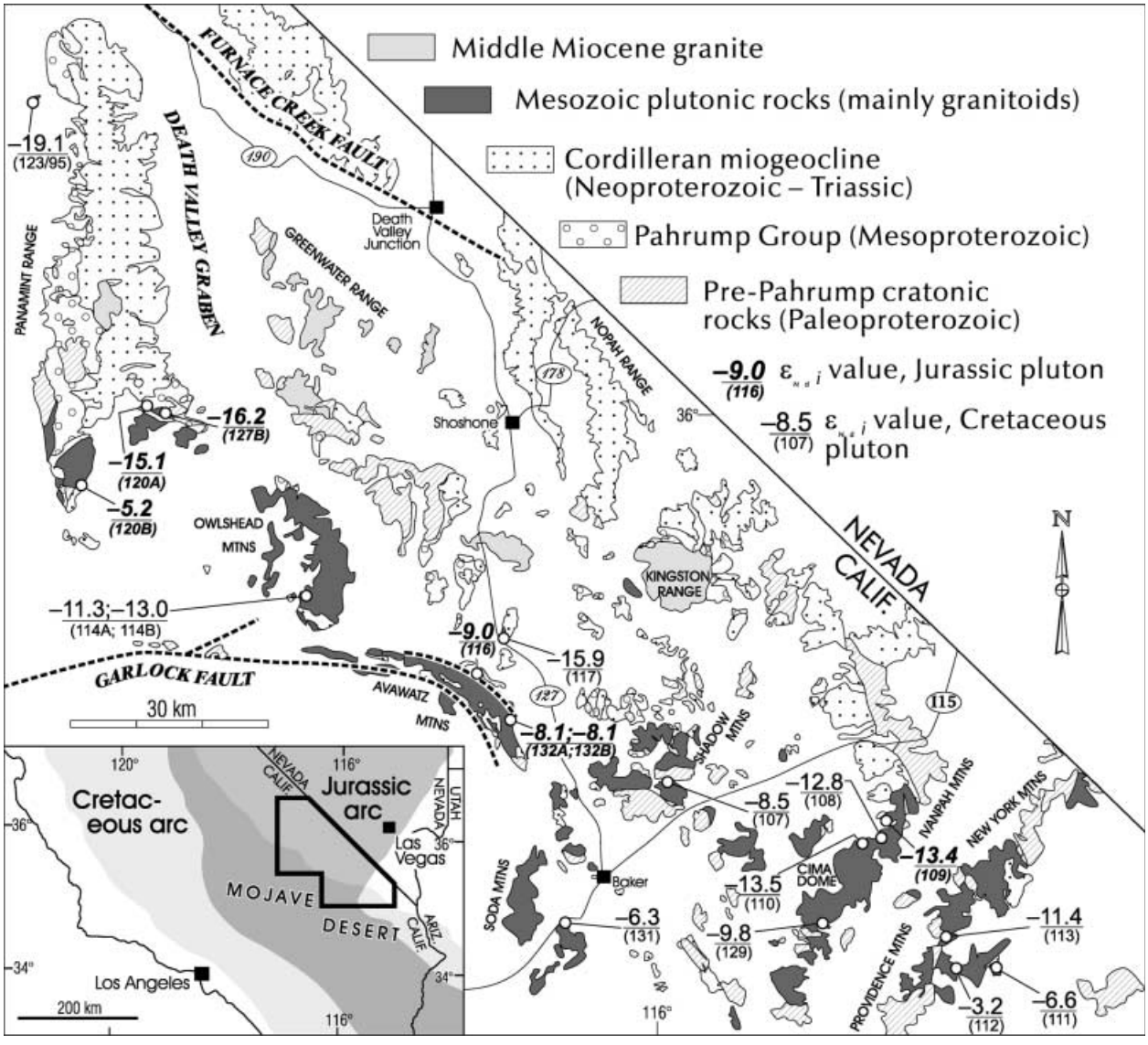

Table 1. Location, modal composition, and age of the Mesozoic plutons sampled from the southern Death Valley region

Sample name	Rock type[a]	Sample location (Lat. °N/long. °W)	Q[b]	A[b]	P[b]	Age (Ma)[c]	Age reference
Jurassic plutons							
DVB-109	Leucomonzogranite	Ivanpah Mountains (35°20′26″/115°40′36″)	0.314	0.356	0.330	145	US Geological Survey (1991)
DVB-116	Biotite–hornblende melagranodiorite	Sheep Canyon (35°34′34″/115°21′16″)	0.264	0.251	0.484	179	DeWitt et al. (1984)
DVB-120A	Granodiorite porphyry	Warm Springs Canyon (35°58′47″/116°58′50″)	0.258[d] (0.021	0.225[d] 0.000	0.517[d] 0.979)	149	Armstrong and Suppe (1973)
DVB-120B	Monzogranite porphyry	Goler Wash (35°51′35″/117°06′15″)	0.246[d] (0.082	0.296[d] 0.000	0.458[d] 0.918)	140	Armstrong and Suppe (1973)
DVB-127B	Biotite tonalite	Warm Springs Canyon (35°58′50″/116°57′30″)	0.331	0.062	0.607	153	Armstrong and Suppe (1973)
DVB-132A	Hornblende–biotite melagranodiorite	Old Mormon Springs (35°30′47″/116°15′30″)	0.284	0.172	0.544	179	Inferred
DVB-132B	Biotite–hornblende melaquartz diorite dike	Old Mormon Springs (35°30′47″/116°15′30″)	0.147	0.004	0.849	≤ 179	Inferred
Cretaceous plutons							
DVB-107	Biotite monzogranite	Halloran Hills (35°24′22″/115°56′43″)	0.243	0.346	0.411	97	DeWitt et al. (1984)
DVB-108	Biotite monzogranite	Kessler Springs (35°18′58″/115°33′03″)	0.241	0.375	0.384	93	Beckerman et al. (1982)
DVB-110	Quartz alkali feldspar syenite	Teutonia Peak (35°18′55″/115°34′56″)	0.109	0.884	0.007	97	DeWitt et al. (1984)
DVB-111	Hornblende–biotite melagranodiorite	Rock Spring (35°09′16″/115°19′55″)	0.222	0.152	0.626	97	US Geological Survey (1991)
DVB-112	Biotite–hornblende gabbro	Black Canyon (35°07′13″/115°24′05″)	0.0	0.0	1.0	≤ 93	E. DeWitt, personal communication (2000)
DVB-113	Biotite leucomonzogranite	Mid Hills (35°09′50″/115°26′37″)	0.297	0.257	0.446	93	US Geological Survey (1991)
DVB-114A	Biotite–hornblende leucoquartz monzonite	Owlshead Mountains (35°40′36″/116°40′05″)	0.179	0.478	0.343	95	R.J. Fleck, personal communication (1977)
DVB-114B	Hornblende–biotite granodiorite dike	Owlshead Mountains (35°40′36″/116°40′05″)	0.385	0.132	0.483	≤ 95	Inferred
DVB-117	Biotite leucomonzogranite	Salt Spring Hills (35°38′10″/116°16′30″)	0.365	0.302	0.333	95	Inferred
DVB-123/95	Two-mica granodiorite	Panamint Range (36°25′49″/117°11′26″)	0.525	0.115	0.360	70	Inferred
DVB-129	Hornblende–biotite monzogranite	Cima Dome SW (35°11′18″/115°35′47″)	0.325	0.251	0.424	97	DeWitt et al. (1984)
DVB-131	Biotite alkali feldspar granite	Zzyzx (35°11′38″/116°08′35″)	0.358	0.642	0.000	95	Inferred

[a]Rock types according to the IUGS classification (Le Maitre 1989)
[b]Modal amounts (normalized to 100%) of quartz (*Q*), alkali feldspar (*A*), and plagioclase (*P*). Determined from thin sections and, for coarse-grained rocks, from stained slabs using the computer scan method of Elliott (1999) – for the two porphyries, see footnote *d*. Numbers in parentheses are for phenocryst assemblages
[c]Based mainly on K–Ar, Ar–Ar, and U–Pb data and geological inference (when age reference is not given)
[d]CIPW normative proportions of quartz (*Q*), orthoclase (*A*), and plagioclase (*P*)

scattered throughout the region. The oldest Jurassic pluton sampled for this study is the 179-Ma Avawatz Mountains quartz monzodiorite. Our two samples of this pluton consist of porphyritic granodiorite from Sheep Canyon (DVB-116) and medium-grained equigranular granodiorite from Old Mormon Springs (DVB-132A); the granodiorite from Old Mormon Springs is intruded by medium-grained quartz diorite dikes (DVB-132B). Other Jurassic plutons within this region are medium-grained equigranular tonalite (DVB-127B) and granodiorite porphyry (DVB-120A) from Warm Springs Canyon in the southern Panamint Range,

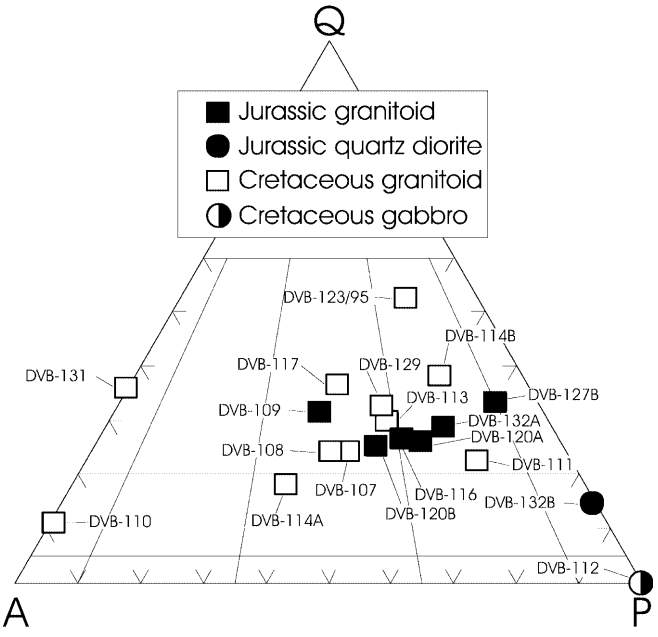

Fig. 2. Modal composition of the 19 Mesozoic plutonic rocks from the southern Death Valley region shown in a Q-A-P diagram (IUGS classification, Le Maitre 1989)

the medium-grained equigranular Ivanpah monzogranite (DVB-109) from the Ivanpah Mountains, and the monzogranite porphyry of Manly Peak (DVB-120B) collected in Goler Wash in the southwestern Panamint Range (Fig. 1). These plutons are Middle to Late Jurassic with ages ranging from 153 to 140 Ma (Table 1) and are often characterized by subvolcanic textures, but are unaffected by sodium metasomatism that is characteristic of subvolcanic Jurassic plutons in the eastern Mojave Desert (see Fox and Miller 1990; Young et al. 1992).

The Cretaceous samples are more felsic and heterogeneous than the sampled Jurassic granitoids. The Teutonia batholith (Beckerman et al. 1982), the largest Cretaceous batholith within the southern Death Valley region, covers approximately 3,000 km^2 and consists of several plutons that vary in composition from quartz syenite to gabbro. These are the 97-Ma Rock Spring granodiorite (DVB-111), Teutonia quartz monzonite, and Halloran Hills monzogranite (DVB-107), as well as the 93-Ma Kessler Springs and Mid Hills monzogranites (DVB-108 and DVB-113, respectively). The Rock Spring granodiorite, Teutonia quartz monzonite, and Kessler Springs monzogranite are porphyritic with feldspar phenocrysts 2–3 cm long; monzogranites in the Halloran Hills and Mid Hills are medium grained and equigranular. The Teutonia quartz monzonite varies in composition from syenogranite to quartz monzonite (Beckerman et al. 1982); our samples from this pluton consist of porphyritic quartz syenite from Teutonia Peak (DVB-110) and coarse-grained equigranular monzogranite south of Cima Dome (DVB-129). The equigranular Black Canyon gabbro (DVB-112) intrudes the Mid Hills monzogranite and is characterized by abundant mafic enclaves. Other Cretaceous plutons within the region include 95-Ma medium-grained equigranular quartz monzonite and granodiorite dikes in the Owlshead Mountains (DVB-114A and DVB-114B, respectively), medium- to coarse-grained monzogranite in the Salt Spring Hills (DVB-117) and granite in the Soda Mountains near Zzyzx (DVB-131), and the porphyritic 70-Ma Skidoo granodiorite (Applegate et al. 1992; Mahood et al. 1996) in the northern Panamint Range.

Analytical methods

Two- to four-kilogram chunks of least-weathered rock were sampled from each locality. From 0.5–1.0 kg of this was crushed and chip edges with signs of weathering, if any, were cut off. The rock chips were then washed in an ultrasonic bath and milled in an iron pan in a swing mill. Two identical splits of sample powder were collected, one for elemental geochemistry and one for radiogenic isotopes.

The major and trace element composition of the samples was determined at the X-Ray Assay Laboratories in Toronto, Canada, in 1998. Concentrations of major elements, Rb, Sr, Zr, Nb, Ba, Cr, Ni, Ga, and Pb were measured by X-ray fluorescence spectrometry using pressed pellets. Rare earth elements, Y, Th, and U were determined on a VG PlasmaQuad inductively coupled plasma/mass spectrometer using a Na_2O_2 fusion technique.

Nd, Sr, and Pb isotopic composition of the samples was determined by O.T.R. at the Unit for Isotope Geology, Geological Survey of Finland, in 1997–1998. Powders from the 17 silicic rocks (approximately 200 mg) were dissolved for a minimum of 2 days in a Teflon bomb at 170 °C in a 1:4 mixture of HF-HNO_3. Powders from the two mafic rocks (250–300 mg) were dissolved in molded Teflon vials for 2 days. After evaporation, the samples were dissolved in HCl and clear solutions thus obtained were spiked with ^{149}Sm–^{150}Nd (all 19 samples) and ^{87}Rb–^{84}Sr (five samples) tracers. Rb, Sr, Nd, and Sm were separated from the same dissolved sample fraction. Pb was purified according to the anion exchange–anodic electrode position procedure (Gulson and Mizon 1979). Rb, Sr, and the light rare earth elements were separated using standard cation exchange chromatography and Sm and Nd were purified on quartz columns according to the method described by Richard et al. (1976). The total procedural blanks were < 100 pg for Nd, < 1 ng for Sr, and < 3 ng for Pb.

Isotopic ratios of Sm, Nd, Sr, and Pb were measured using a seven-collector VG SECTOR 54 mass spectrometer (those of Nd and Sr in dynamic mode). Isotopic measurements on Rb were performed on a non-commercial Nier-type mass spectrometer built at the Geological Survey of Finland. Isotopic ratios of Nd were normalized to $^{146}Nd/^{144}Nd = 0.7219$. Repeated analyzes of the La Jolla Nd standard gave $^{143}Nd/^{144}Nd$ of 0.511850 ± 0.000011 (mean and external 2σ error of 13 measurements). The external (2σ) precision of the measured ^{143}Nd–^{144}Nd ratios is thus better than 0.0025%. Based on duplicate analyses, the Sm–Nd ratios are estimated to be accurate within 0.5%. The maximum error in the ϵ_{Nd} values is ± 0.35 ϵ-units. Isotopic ratios of Sr were normalized to $^{86}Sr/^{88}Sr = 0.1194$. Repeated analyses of the NBS 987 Sr standard yielded $^{87}Sr/^{86}Sr$ of 0.710259 ± 0.000014 (mean and external 2σ error of 11 measurements). The external precision (2σ) is thus better than 0.002%. The reported ^{87}Sr–^{86}Sr ratios have been normalized to $^{87}Sr/^{86}Sr = 0.71024$ of the NBS 987 standard. The error in the Rb–Sr ratios determined by isotope dilution is 0.5%, that for ratios based on XRF measurements is 5% (see Tables 2 and 3, footnote b). A mass fractionation correction of $+0.12$ percent per a.m.u. was made to normalize the measured Pb isotopic ratios to the NBS 981 Pb standard ($^{206}Pb/^{204}Pb = 16.937$, $^{207}Pb/^{204}Pb = 15.491$, $^{208}Pb/^{204}Pb = 36.69$; Gulson et al. 1984). External 2σ errors are 0.15% on $^{206}Pb/^{204}Pb$ and $^{207}Pb/^{204}Pb$ and 0.2% on $^{208}Pb/^{204}Pb$. Each reported ratio is the average of two separate mass spectrometer runs.

Table 2. Elemental geochemical and Nd, Sr, and Pb isotopic data for the Mesozoic plutons of the southern Death Valley region

Sample name	Jurassic plutons							Cretaceous plutons	
	DVB-109	DVB-116	DVB-120A	DVB-120B	DVB-127B	DVB-132A	DVB-132B	DVB-107	DVB-108
SiO_2 (wt%)	76.5	58.5	66.5	66.7	60.7	63.6	52.3	68.5	67.9
TiO_2	0.035	0.942	0.542	0.321	0.728	0.653	1.728	0.431	0.416
Al_2O_3	12.3	16.0	15.8	14.7	16.9	15.1	15.6	14.7	15.4
Fe_2O_3	1.25	7.94	4.41	2.54	5.87	6.53	10.90	3.01	3.19
MnO	0.03	0.13	0.08	0.05	0.10	0.11	0.16	0.04	0.06
MgO	0.03	3.17	1.46	0.55	2.18	2.38	4.84	0.99	1.15
CaO	0.29	5.47	4.15	3.60	5.87	4.89	7.72	2.41	3.11
Na_2O	3.79	2.68	3.12	3.40	2.95	2.51	3.27	3.60	4.40
K_2O	5.03	3.68	3.35	4.43	2.67	4.03	2.09	4.27	3.47
P_2O_5	0.03	0.23	0.14	0.16	0.22	0.19	0.52	0.13	0.17
LOI	0.30	0.45	0.40	2.90	0.45	0.30	0.60	0.95	0.35
Total	99.59	99.19	99.95	99.35	98.64	100.29	99.73	99.03	99.62
A/CNK[a]	1.01	0.87	0.97	0.87	0.92	0.87	0.72	0.98	0.93
Ga (ppm)	17	18	17	16	19	16	18	20	
Ba	< 20	1,050	824	1,180	526	928	1,210	599	718
Nb	40	8	10	11	10	14	40	12	9
La	16.9	31.3	40.4	57.1	32.4	49.3	32.8	44.6	43.8
Ce	28.8	51.9	68.8	91.6	65.9	93.3	74.4	67.1	64.1
Pr	5.6	7.9	10.3	12.1	7.4	10.0	9.3	8.0	8.7
Eu	0.12	1.65	1.65	1.43	1.57	1.35	2.26	0.99	1.21
Gd	11.90	5.00	6.50	3.80	5.90	6.50	8.20	3.20	3.60
Tb	2.30	0.60	1.00	0.50	0.90	1.00	1.10	0.40	0.40
Dy	16.50	4.00	5.60	2.60	4.70	4.80	6.00	2.20	2.30
Ho	3.62	0.80	1.10	0.47	1.04	0.99	1.23	0.42	0.40
Er	13.0	2.6	3.8	1.6	2.9	2.9	3.4	1.4	1.3
Tm	2.7	0.4	0.6	0.3	0.5	0.4	0.4	0.2	0.2
Yb	15.5	2.3	3.4	1.4	3.4	3.2	3.6	1.2	1.2
Lu	2.12	0.31	0.47	0.18	0.31	0.25	0.29	0.18	0.18
Y	134	18	27	13	33	35	44	13	14
Zr	80	261	257	186	294	182	815	155	163
Age (Ma)	145	179	149	140	153	179	179	97	93
Sm (ppm)[b]	8.241	3.948	6.211	5.364	6.457	7.156	8.891	3.315	4.208
Nd (ppm)[b]	20.89	18.63	33.36	35.80	32.93	39.45	44.31	20.36	26.19
$^{147}Sm/^{144}Nd$	0.2385	0.1281	0.1125	0.09058	0.1185	0.1097	0.1213	0.09843	0.09714
$^{143}Nd/^{144}Nd$[c]	0.511991 (14)	0.512098 (9)	0.511780 (11)	0.512271 (11)	0.511731 (11)	0.512122 (8)	0.512138 (9)	0.512142 (11)	0.511926 (12)
ϵ_{Nd}[d,e]	–13.4	–9.0	–15.1	–5.3	–16.2	–8.1	–8.0	–8.5	–12.8
T_{DM}(Ga)[d]	–	1.67	1.90	0.96	2.09	1.35	1.49	1.19	1.46
Rb (ppm)[b]	567.9	140	111	109	101.6	165	70.58	191	104
Sr (ppm)[b]	3.245	537	227	512	283.4	457	547.7	338	687
$^{87}Rb/^{86}Sr$	567.9	0.7539	1.416	0.6163	1.040	1.045	0.3729	1.635	0.4379
$^{87}Sr/^{86}Sr$[c]	1.95436 (7)	0.710492 (14)	0.722128 (14)	0.708355 (14)	0.728012 (15)	0.710887 (13)	0.710207 (13)	0.711367 (14)	0.710675 (14)
$^{87}Sr/^{86}Sr_i$[e,f]	0.78385 (0.00585)	0.70858 (0.00010)	0.71913 (0.00015)	0.70713 (0.00006)	0.72575 (0.00001)	0.70823 (0.00013)	0.70926 (< 0.00001)	0.70911 (0.00011)	0.71010 (0.00003)
Pb (ppm)[b]	33	14	20	25	9	15	24	15	18
Th (ppm)[b]	44.0	35.6	45.3	16.6	9.4	64.4	4.2	30.6	36.2
U (ppm)[b]	5.4	2.0	1.8	4.6	1.6	16.7	0.9	4.2	2.0
$^{206}Pb/^{204}Pb$[c]	17.698	18.251	18.350	18.922	20.258	20.625	18.165	18.268	17.937
$^{207}Pb/^{204}Pb$[c]	15.544	15.594	15.630	15.647	15.829	15.707	15.588	15.577	15.569
$^{208}Pb/^{204}Pb$[c]	39.245	39.395	39.751	39.163	40.551	41.563	39.341	39.846	39.211
$^{206}Pb/^{204}Pb_i$[e]	17.46	17.99	18.21	18.66	19.97	18.49	18.10	17.99	17.83
$^{207}Pb/^{204}Pb_i$[e]	15.53	15.58	15.62	15.63	15.82	15.60	15.58	15.56	15.56
$^{208}Pb/^{204}Pb_i$[e]	38.63	37.91	38.66	38.86	40.01	38.94	39.24	39.21	38.60

[a] $Al_2O_3/(CaO + Na_2O + K_2O)$, atomic

[b] Sm and Nd by ID/MS; Rb and Sr by ID/MS when four significant digits, otherwise by XRF; Pb by XRF; Th and U by ICP/MS

[c] $^{143}Nd/^{144}Nd$ and $^{87}Sr/^{86}Sr$ normalized to $^{146}Nd/^{144}Nd = 0.7219$ and $^{84}Sr/^{86}Sr = 0.1194$, respectively; numbers in parentheses are $2\sigma_m$ in the last significant digits; Pb isotopic ratios reported relative to the NBS 981 standard

[d] Chondritic values used to calculate ϵ_{Ndi} were $^{143}Nd/^{144}Nd = 0.512638$ and $^{147}Sm/^{144}Nd = 0.1966$; T_{DM} is depleted mantle model age (DePaolo 1981b)

[e] Initial ratios calculated using the given elemental concentrations and ages

[f] Reported errors in parentheses include uncertainty in $^{87}Rb/^{86}Sr$

Table 3. Elemental geochemical and Nd, Sr, and Pb isotopic data for the Mesozoic plutons of the southern Death Valley region

Sample name	Cretaceous plutons									
	DVB-110	DVB-111	DVB-112	DVB-113	DVB-114A	DVB-114B	DVB-117	DVB-123/95	DVB-129	DVB-131
SiO_2 (wt%)	70.2	60.5	46.6	73.8	65.0	66.8	73.9	69.0	73.1	77.0
TiO_2	0.186	0.893	1.739	0.142	0.447	1.021	0.166	0.245	0.304	0.11
Al_2O_3	14.3	16.6	18.2	13.6	16.2	13.7	13.7	15.4	13.2	12.0
Fe_2O_3	1.50	6.46	10.10	1.46	4.47	6.09	2.22	2.60	2.27	1.18
MnO	0.03	0.12	0.21	0.02	0.14	0.10	0.06	0.05	0.07	0.07
MgO	0.29	2.92	6.90	0.40	0.40	1.34	0.28	0.66	0.88	0.04
CaO	1.05	5.68	10.40	1.90	1.32	3.33	1.69	3.03	1.80	0.24
Na_2O	2.21	3.72	2.76	3.58	4.74	2.97	3.67	4.11	3.50	4.25
K_2O	9.23	2.77	0.85	4.20	6.04	3.70	3.94	2.62	3.88	4.52
P_2O_5	0.09	0.26	0.36	0.05	0.12	0.35	0.04	0.13	0.16	–0.01
LOI	0.10	0.10	1.20	0.15	0.15	0.40	0.35	1.40	0.30	0.05
Total	99.19	100.02	99.32	99.30	99.03	99.80	100.02	99.25	99.46	99.45
A/CNK[a]	0.92	0.85	0.75	0.98	0.97	0.92	1.02	1.02	1.00	0.97
Ga (ppm)	13	19	18	25	16	15	20	15	18	
Ba	897	849	456	413	1,240	1,210	698	641	685	23
Nb	9	9	9	2	49	14	12	8	15	23
La	125	28.5	18.9	12.6	39.3	52.6	42.4	49.8	21.1	28.2
Ce	211.0	50.0	38.9	18.3	88.3	99.7	70.7	83.8	39.9	54.6
Pr	29.6	7.6	7.1	2.6	16.9	14.9	10.2	11.1	4.4	5.5
Eu	1.59	1.55	1.94	0.52	1.67	2.56	1.09	1.38	0.73	0.17
Gd	10.90	5.00	7.00	1.10	28.50	10.20	6.20	3.50	2.60	3.70
Tb	1.70	0.70	1.10	0.10	5.60	1.70	1.00	0.50	0.40	0.70
Dy	9.40	3.80	5.80	0.60	35.40	8.70	5.70	2.20	1.90	4.20
Ho	1.69	0.71	1.18	0.07	7.55	1.72	1.25	0.32	0.39	0.93
Er	5.8	2.6	3.7	0.4	24.2	5.6	4.2	1.0	1.1	3.2
Tm	0.9	0.4	0.6	0.1	3.9	0.9	0.8	0.2	0.2	0.5
Yb	4.6	2.3	2.9	0.4	19.1	4.6	4.4	0.8	1.9	4.4
Lu	0.56	0.28	0.45	0.09	2.28	0.61	0.56	0.09	< 0.05	0.38
Y	40	18	27	3	176	42	32	9	20	40
Zr	142	177	117	83	841	408	143	191	114	148
Age (Ma)	97	97	93	93	95	95	95	70	97	95
Sm (ppm)[b]	12.04	3.819	6.138	0.998	21.21	10.50	5.756	5.372	3.577	4.398
Nd (ppm)[b]	78.47	17.56	26.81	6.851	64.95	54.03	31.47	36.15	19.59	21.21
$^{147}Sm/^{144}Nd$	0.09274	0.1315	0.1384	0.08806	0.1974	0.1175	0.1106	0.08982	0.1104	0.1254
$^{143}Nd/^{144}Nd$[c]	0.511882	0.512259	0.512436	0.511990	0.512061	0.511926	0.511773	0.511611	0.512081	0.512273
	(11)	(7)	(8)	(14)	(11)	(8)	(12)	(10)	(8)	(10)
ϵ_{Ndi}[d,e]	–13.5	–6.6	–3.2	–11.4	–11.3	–13.0	–15.9	–19.1	–9.8	–6.3
T_{DM}(Ga)[d]	1.46	1.45	1.23	1.28	n.a.	1.76	1.87	1.76	1.41	1.33
Rb (ppm)[b]	201	94.72	19.21	104	195	101	147	98	154	188
Sr (ppm)[b]	135	497.1	636.5	424	61	251	118	41	324	5
$^{87}Rb/^{86}Sr$	4.314	0.5512	0.08729	0.7098	9.271	1.166	3.608	6.924	1.375	111.8
$^{87}Sr/^{86}Sr$[c]	0.722992	0.708202	0.706085	0.710527	0.732143	0.724846	0.727174	0.721336	0.711022	0.974225
	(12)	(13)	(11)	(14)	(16)	(13)	(15)	(14)	(14)	(21)
$^{87}Sr/^{86}Sr^{i}$[e,f]	0.71705	0.70744	0.70597	0.70959	0.71963	0.72327	0.72230	0.71445	0.70913	0.82336
	(0.00030)	(< 0.00001)	(< 0.00001)	(0.00005)	(0.00063)	(0.00008)	(0.00024)	(0.00034)	(0.00009)	(0.00755)
Pb (ppm)[b]	23	7	11	16	35	13	17	17	18	15
Th (ppm)[b]	30.6	18.5	5.7	18.1	24.0	27.8	21.4	14.2	7.1	11.9
U (ppm)[b]	4.2	2.0	0.5	1.6	5.4	1.3	2.5	1.7	1.2	1.8

Table 3. Continued

Sample name	Cretaceous plutons									
	DVB-110	DVB-111	DVB-112	DVB-113	DVB-114A	DVB-114B	DVB-117	DVB-123/95	DVB-129	DVB-131
$^{206}Pb/^{204}Pb^{c}$	17.574	17.889	17.729	17.871	18.530	18.546	18.410	17.842	18.134	18.735
$^{207}Pb/^{204}Pb^{c}$	15.549	15.544	15.542	15.561	15.648	15.659	15.629	15.563	15.574	15.625
$^{208}Pb/^{204}Pb^{c}$	39.549	39.284	39.037	39.085	39.667	39.618	39.750	40.039	39.352	39.456
$^{206}Pb/^{204}Pb_{i}^{e}$	17.40	17.61	17.69	17.78	18.38	18.45	18.27	17.77	18.07	18.62
$^{207}Pb/^{204}Pb_{i}^{e}$	15.54	15.53	15.54	15.56	15.64	15.66	15.62	15.56	15.57	15.62
$^{208}Pb/^{204}Pb_{i}^{e}$	39.14	38.47	38.88	38.75	39.45	38.95	39.36	39.85	39.23	39.21

[a] $Al_2O_3/(CaO + Na_2O + K_2O)$, atomic
[b] Sm and Nd by ID/MS; Rb and Sr by ID/MS when four significant digits, otherwise by XRF; Pb by XRF; Th and U by ICP/MS
[c] $^{143}Nd/^{144}Nd$ and $^{87}Sr/^{86}Sr$ normalized to $^{146}Nd/^{144}Nd = 0.7219$ and $^{84}Sr/^{86}Sr = 0.1194$, respectively; numbers in parentheses are $2\sigma_m$ in the last significant digits; Pb isotopic ratios reported relative to the NBS 981 standard
[d] Chondritic values used to calculate ϵ_{Nd}; were $^{143}Nd/^{144}Nd = 0.512638$ and $^{147}Sm/^{144}Nd = 0.1966$; T_{DM} is depleted mantle model age (DePaolo 1981b)
[e] Initial ratios calculated using the given elemental concentrations and ages
[f] Reported errors in parentheses include uncertainty in $^{87}Rb/^{86}Sr$

Major and trace element geochemistry

Geochemical composition of Jurassic and Cretaceous plutons in the southern Death Valley region is listed in Tables 2 and 3 and shown in Figs. 3, 4, and 5. We describe the major and trace element geochemistry as well as the isotopic composition of the granitoid rocks separate from the mafic rocks.

Granitoid rocks

Harker variation diagrams of Jurassic and Cretaceous granitoid rocks are shown in Fig. 3a–h. The Jurassic granitoids contain 58.5 to 76.5 wt% SiO_2 (mean 65.4%); the Cretaceous samples yield 60.5 to 77% SiO_2 (mean 69.6%). The Jurassic samples contain, on average, more FeO_{tot}, MgO, TiO_2, P_2O_5, Al_2O_3, and CaO than the Cretaceous samples. Cretaceous quartz monzonite in the Owlshead Mountains contains very little CaO (Fig. 3f) whereas the granodiorite dike that cuts the quartz monzonite yields anomalously high TiO_2 and P_2O_5 contents. The Jurassic granitoids contain 2.5–3.8% Na_2O (mean 3.1%) and 2.7–5.0% K_2O (mean 3.9%); Cretaceous granitoids yield 2.2–4.7% Na_2O (mean 3.7%) and 2.6–9.2% K_2O (mean 4.2%, Fig. 3g, h). The Teutonia quartz syenite yields the greatest K_2O (9.2%) and least Na_2O (2.2%) content and an anomalously high K/Na (4.2 as opposed to ~1 in the other granitoid samples).

Most of the Jurassic and Cretaceous granitoid samples are subalkalic and calc-alkaline (Fig. 4). Except for the Ivanpah monzogranite, the Jurassic granitoids yield lower values and less variation in $FeO_{tot}/(FeO_{tot} + MgO)$ than the Cretaceous granitoids. The Owlshead monzogranite and Teutonia quartz syenite are alkalic; the Owlshead monzogranite as well as the Salt Spring Hills monzogranite and Zzyzx granite are tholeiitic. Overall, the Cretaceous samples are somewhat more aluminous in character than the Jurassic granitoids (Fig. 4b). The Skidoo granodiorite has the largest A/CNK of the Cretaceous granites with similar silica contents (~70%).

Variation of selected trace elements in the Jurassic and Cretaceous granitoids are shown in Fig. 3i–p. Rb varies in both suites from ~100 to 200 ppm, save for the Ivanpah monzogranite with nearly 570 ppm Rb (Fig. 3i). Sr concentrations from Cretaceous granitoids are more variable and span a somewhat larger range (5–687 ppm) than Jurassic granitoids (3–537 ppm; Fig. 3j). Ba also shows considerable scatter (< 20–1,180 ppm in the Jurassic samples; 23–1,240 ppm in Cretaceous). In general, Zr concentrations in the Jurassic samples (~200–

►

Fig. 3. Harker and trace element variation diagrams showing the variation of **a** total iron as FeO, **b** MgO, **c** TiO_2, **d** P_2O_5, **e** Al_2O_3, **f** CaO, **g** Na_2O, **h** K_2O, **i** Rb, **j** Sr, **k** Ba, **l** Zr, **m** U, **n** Th, **o** Pb, and **p** Ce in the Mesozoic plutons of the southern Death Valley region. Major elements in wt%, trace elements in ppm

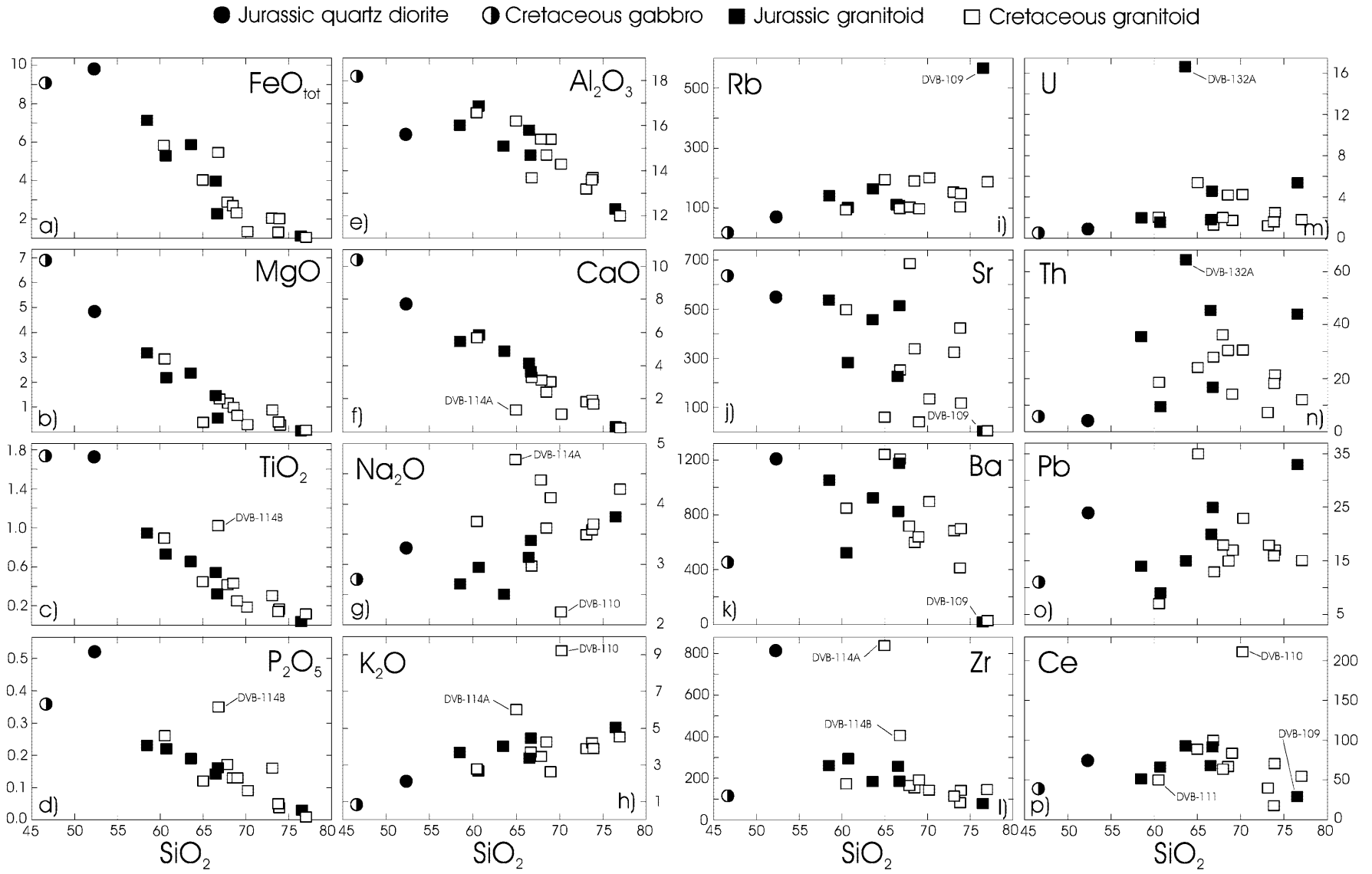
Jurassic quartz diorite
Cretaceous gabbro
Jurassic granitoid
Cretaceous granitoid
FeOtot
Al2O3
Rb
U
MgO
CaO
Sr
Th
TiO2
Na2O
Ba
Pb
P2O5
K2O
Zr
Ce
SiO2
DVB-109
DVB-132A
DVB-114A
DVB-114B
DVB-110
DVB-111

300 ppm) are greater than in the Cretaceous samples (~100–200 ppm). Samples from the Owlshead Mountains, however, have much greater Zr concentrations than any other sample at similar SiO_2 (Fig. 3l). U and Th concentrations are similar in both granitoid suites; granodiorite from Old Mormon Springs, however, yields anomalously high concentrations of U and Th (Fig. 3m, n). Pb shows a fairly consistent trend (9–33 ppm) for the Jurassic samples, but is more variable in the Cretaceous samples (Fig. 3o). Ce is between ~20 and 100 ppm in both the Jurassic and the Cretaceous granitoids, save for the Cretaceous Teutonia quartz syenite (Fig. 3p).

Chondrite-normalized rare earth element (REE) compositions of the Jurassic and Cretaceous granitoids are shown in Fig. 5. REE patterns of five Jurassic granitoids (Fig. 5a) are smooth and moderately enriched in the light REE (LREE); $(La/Yb)_N$ ranges from 6.4 to 27.5 (mean 12.3) and no distinct Eu anomaly is present. The Ivanpah monzogranite shows an anomalous, LREE-depleted pattern [$(La/Yb)_N = 0.74$] with a deep Eu anomaly ($Eu/Eu^* = 0.04$).

REE patterns from Cretaceous granitoids in the southeastern half of the southern Death Valley region differ from those in the northwestern half of the region (Fig. 5b, c). Kessler Springs monzogranite, Teutonia quartz syenite, and monzogranites from Cima Dome and Halloran Hills show similar degrees of LREE enrichment [mean $(La/Yb)_N = 8.9$] and a small negative Eu anomaly (mean $Eu/Eu^* = 0.76$). The Rock Spring granodiorite is slightly enriched in the LREE [$(La/Yb)_N = 8.4$], but yields no marked Eu anomaly. The Mid Hills monzogranite has a moderately LREE-enriched pattern [$(La/Yb)_N = 21.2$] and a small positive Eu anomaly ($Eu/Eu^* = 1.52$) whereas the Zzyzx granite shows slight enrichment in the LREE [$(La/Yb)_N = 4.32$] and a large Eu anomaly ($Eu/Eu^* = 0.13$). Samples from the Owlshead Mountains and Salt Spring Hills (Fig. 5c), however, are clearly different with less LREE-enriched patterns [$(La/Yb)_N = 1.4$ to 0.76] and larger Eu anomalies ($Eu/Eu^* = 0.21$ to 0.76). The Skidoo granodiorite has the largest $(La/Yb)_N$ (42.0) of our samples and no Eu anomaly (Fig. 5c).

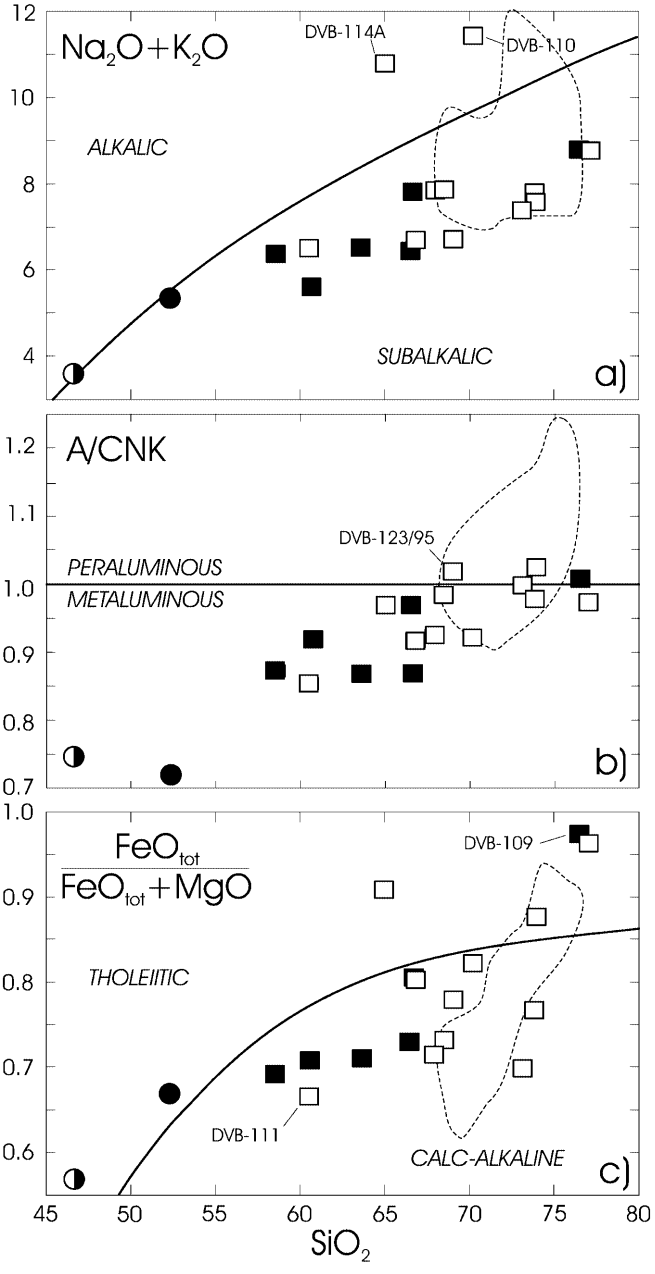

Fig. 4. Composition of the Mesozoic plutons from the southern Death Valley region shown in **a** $Na_2O + K_2O$ vs. SiO_2, **b** A/CNK vs. SiO_2, and **c** $FeO_{tot}/(FeO_{tot} + MgO)$ vs. SiO_2 diagrams. A/CNK in **b** is molecular $Al_2O_3/(CaO + Na_2O + K_2O)$, all other variables in wt%. FeO_{tot} in **c** is total iron reported as FeO. Field boundaries in **a** from Irvine and Baragar (1971) and in **c** from Miyashiro (1974). Sample *symbols* as in Fig. 2. *Dashed fields* represent composition of Cretaceous granitoids of the Teutonia batholith in the southern part of the region (Beckerman et al. 1982)

Mafic rocks

Our most mafic samples are a quartz diorite dike that is synchronous with the Jurassic Avawatz Mountains quartz monzodiorite at Old Mormon Springs, and the Cretaceous Black Canyon gabbro. The quartz diorite dike is more evolved with mg# [atomic Mg/(Mg + 0.85Fe)] of 51 than the gabbro (mg# 61; Tables 2, 3, and 4, Fig. 3). The dike also contains more SiO_2, FeO_{tot}, Na_2O, and K_2O and less CaO than the gabbro (Fig. 3f–h). The gabbro, with 18.2% Al_2O_3, is cumulus-enriched in plagioclase and, thus, does not represent a melt composition. Both mafic rocks straddle the boundary between alkalic and subalkalic fields and are tholeiitic (Fig. 4a, c). The quartz diorite dike contains 0.7% normative quartz, the gabbro is olivine normative (16.2%). The dike also yields higher abundances of Rb, Ba, Zr, Pb, and Ce than the gabbro (Fig. 3). Sr values are 548 ppm in the quartz diorite and 637 ppm in the gabbro (Fig. 3j). Both mafic samples yield moderately LREE-enriched patterns with no marked Eu anomaly (Fig. 5d). The $(La/Yb)_N$ of the quartz diorite and gabbro are 6.14 and 4.39, respectively.

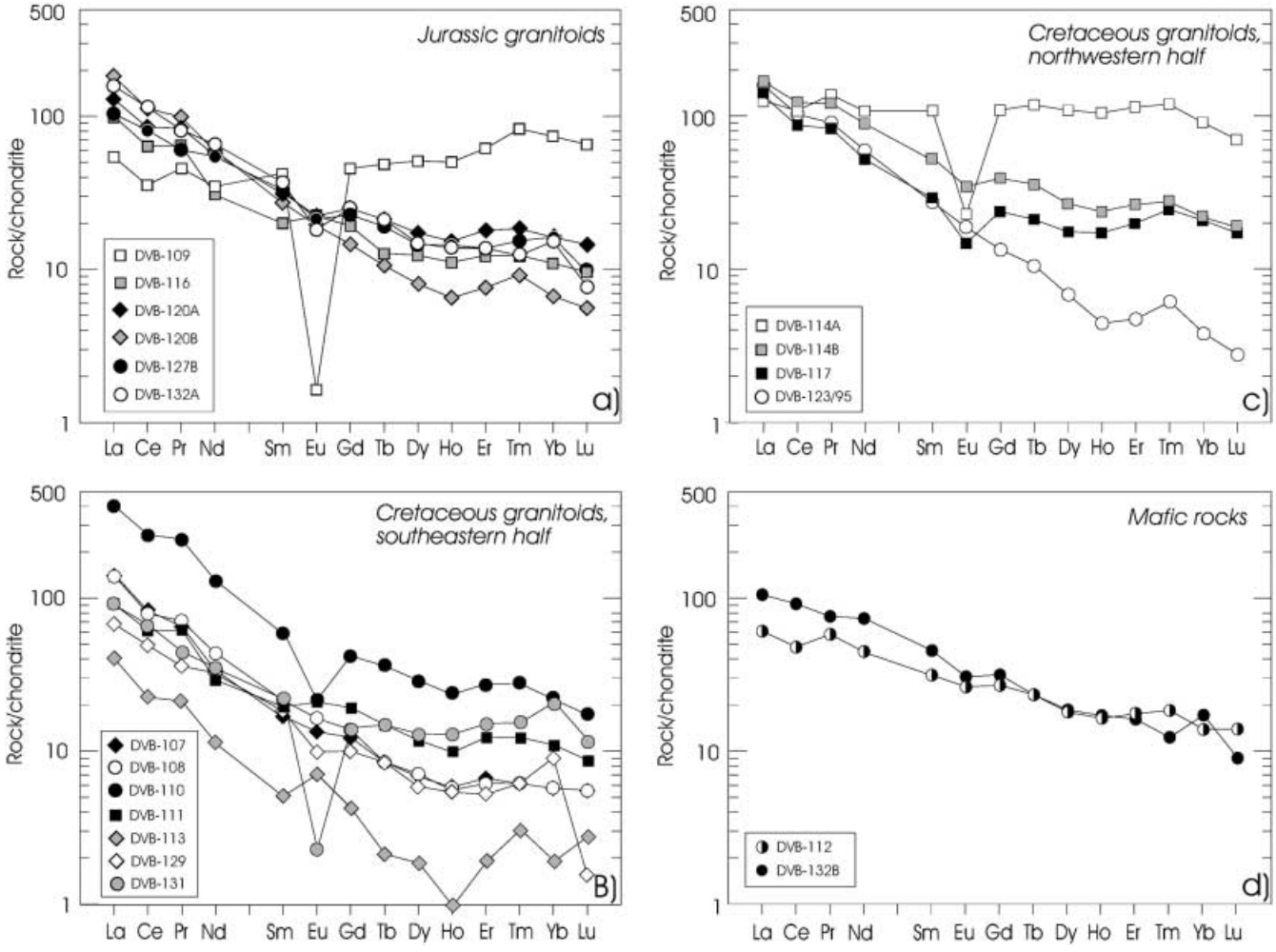

Fig. 5. Rare earth element composition of the **a** Jurassic and **b**, **c** Cretaceous granitoids and **d** Mesozoic mafic rocks of the southern Death Valley region normalized against chondrite (Boynton 1984)

Isotope geochemistry

Nd, Sr, and Pb isotopic compositions of our samples are listed in Tables 2 and 3 and shown in Figs. 6 and 7. For each sample, initial isotopic compositions have been determined and are reported as ϵ_{Ndi}, $^{87}Sr/^{86}Sr_i$, and initial ^{204}Pb-based ratios ($^{206}Pb/^{204}Pb_i$, $^{207}Pb/^{204}Pb_i$, and $^{208}Pb/^{204}Pb_i$).

Granitoid rocks

The five Jurassic granitoid samples with smooth REE patterns have $^{147}Sm/^{144}Nd$ between 0.091 and 0.128 (Tables 2 and 3), but show large variation in the initial

Table 4. Composition of mafic rocks and possible mantle sources, Mojave Desert

	Southern Death Valley region		Central Mojave Desert	Eastern Mojave Desert	
	Gabbro at Black Canyon (93 Ma)	Quartz diorite dike at Old Mormon Springs (179 Ma)	Asthenospheric mantle[a]	Bristol Lake diorites[b]	Cenozoic basalts[c]
SiO_2 (wt%)	46.6	52.3	–	49.4	–
mg#[d]	61	51	–	56	–
ϵ_{Ndi}	–3.2	–8.1	+4	–6.1	<–8
Sr_i	0.7060	0.7093	0.7035	0.7069	>0.707
$^{206}Pb/^{204}Pb_i$	17.69	18.10	19.05	–	17.8–18.8

[a]Miller and Glazner (1995)
[b]Young et al. (1992)
[c]Farmer et al. (1989)
[d]Mg/(Mg + 0.85*Fe), atomic

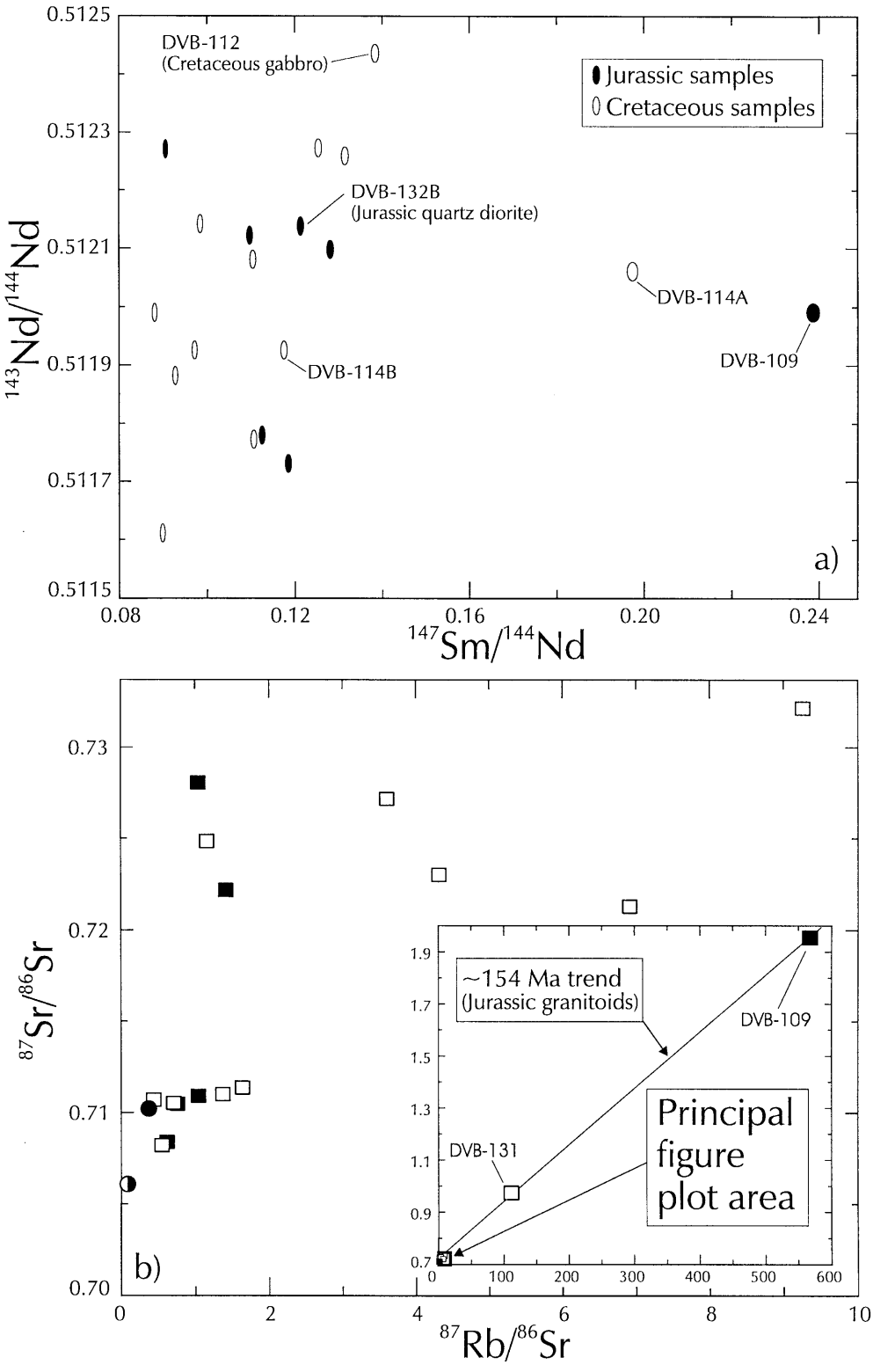

Fig. 6. Isotopic composition of the Mesozoic plutonic rocks from the southern Death Valley region shown in **a** $^{143}Nd/^{144}Nd$ vs. $^{147}Sm/^{144}Nd$ and **b** $^{87}Sr/^{86}Sr$ vs. $^{87}Rb/^{86}Sr$ diagram. The size of the *symbols* in **a** is proportional to the 2σ errors of the variables. *Inset* in **b** shows the entire data range of the 19 samples. *Symbols* in **b** as in Fig. 2

compositions; ϵ_{Ndi} values range from –5.3 (monzogranite porphyry of Manly Peak) to –16.2 (Warm Springs tonalite). Nd model ages (T_{DM}, calculated according to DePaolo 1981b) show considerable variation, 0.96–2.09 Ga, and are older than the crystallization ages of the plutons. The Ivanpah monzogranite with anomalous REE budget (Fig. 5a) yields a high $^{147}Sm/^{144}Nd$ (0.239) and, thus, no meaningful model age.

$^{147}Sm/^{144}Nd$ of the Cretaceous granitoids vary from 0.088 to 0.132, except for the Owlshead quartz monzonite (0.1974). ϵ_{Ndi} are between –6.3 (Zzyzx granite) and –19.1 (Skidoo granodiorite), thus spanning a

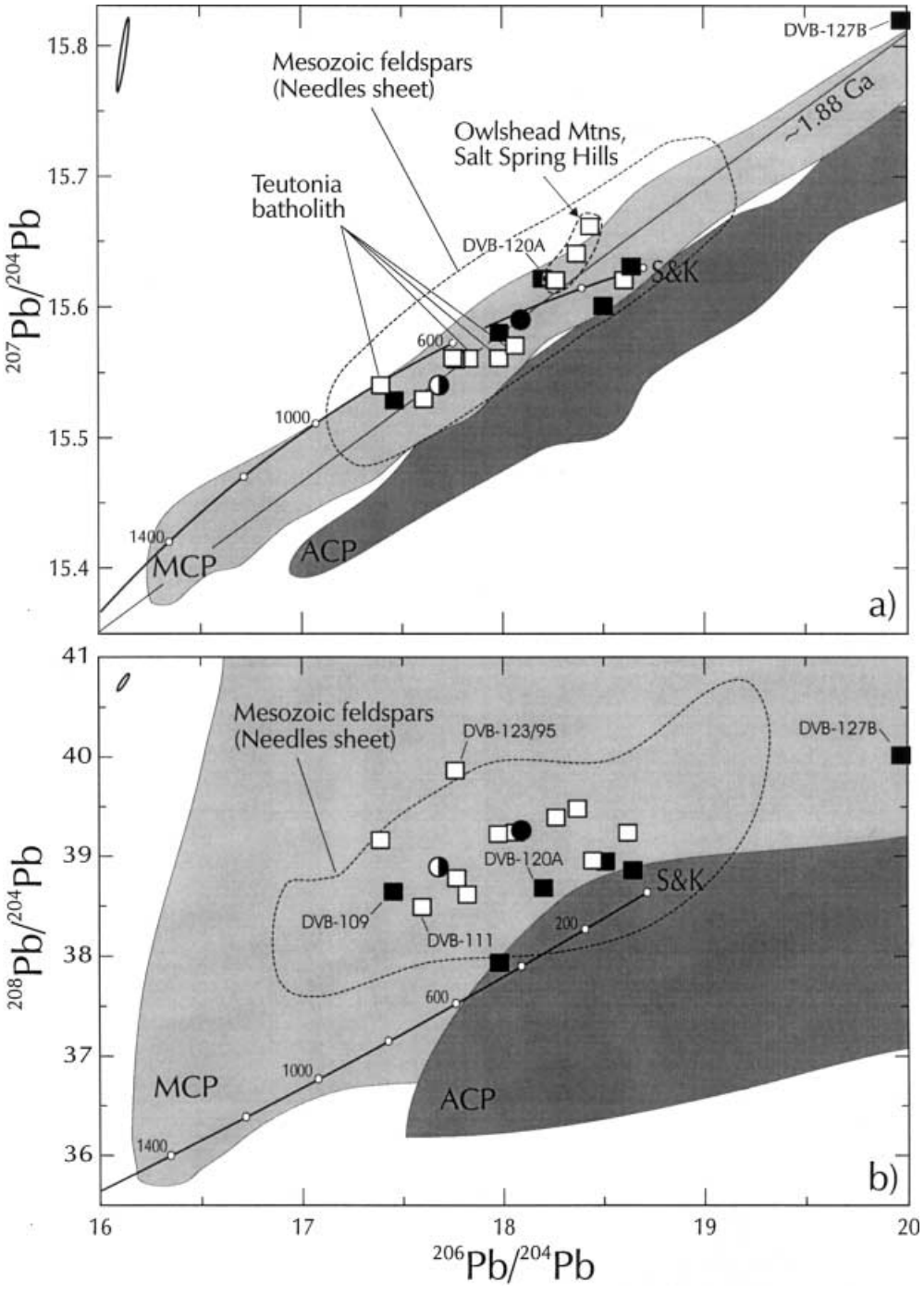

Fig. 7. Initial Pb isotopic composition of the Mesozoic rocks from the southern Death Valley region shown in **a** $^{207}Pb/^{204}Pb$ vs. $^{206}Pb/^{204}Pb$ and **b** $^{208}Pb/^{204}Pb$ vs. $^{206}Pb/^{204}Pb$ diagrams. Growth curves for average crustal Pb (*S&K*, Stacey and Kramers 1975) are shown, as are fields for the Mesozoic feldspars from southeastern California (Wooden et al. 1988) and the Precambrian Mojave (*MCP*) and Arizona (*ACP*) crustal provinces (Wooden and Miller 1990). 2σ error ellipses are shown in the *upper left corners* of **a** and **b**. *Symbols* as in Fig. 2

slightly wider range than the Jurassic plutons. T_{DM} of the Cretaceous granitoids vary from 1.19 to 1.87 Ga. Like the Jurassic granitoids, the Nd ratios of the Cretaceous samples are extremely varied and do not provide meaningful chronological information (Fig. 6a).

The Jurassic granitoids have relatively low $^{87}Rb/^{86}Sr$ and $^{87}Sr/^{86}Sr$; most of them plot on the extreme left side of the Rb–Sr isochron diagram (Fig. 6b). Calculated $^{87}Sr/^{86}Sr_i$ vary from 0.7071 (monzogranite porphyry of Manly Peak) to 0.7258 (Warm Springs tonalite, Tables 2 and 3). The Ivanpah monzogranite yields very high $^{87}Rb/^{86}Sr$ (568) and $^{87}Sr/^{86}Sr$ (1.954). The Jurassic samples fall on a trend that is controlled by the Ivanpah monzogranite and corresponds to an age of ~154 Ma (Fig. 6b).

With one exception, the Cretaceous granitoids yield roughly similar $^{87}Sr/^{86}Sr$ relative to the Jurassic granitoids (Fig. 6b). The Zzyzx granite yields anomalously high ratios ($^{87}Rb/^{86}Sr = 112$, $^{87}Sr/^{86}Sr = 0.9742$) and falls close to the ~154-Ma trend of the Jurassic granitoids (Tables 2 and 3, Fig. 6b). Save for the Zzyzx granite,

$^{87}Sr/^{86}Sr_i$ of the Cretaceous granitoids vary from 0.7074 (Rock Spring granodiorite) to 0.7233 (granodiorite dike in the Owlshead Mountains).

The Jurassic granitoids yield $^{206}Pb/^{204}Pb_i$ of 17.46 to 19.97, $^{207}Pb/^{204}Pb_i$ of 15.53 to 15.82, and $^{208}Pb/^{204}Pb_i$ of 37.91 to 40.01 (Tables 2 and 3; Fig. 7). The Warm Springs tonalite is the most radiogenic of all the Jurassic and Cretaceous samples. All of the Jurassic samples plot within the Precambrian Mojave crustal province of Wooden and Miller (1990) and, except for the Warm Springs granodiorite, plot roughly along the growth curve of average crustal Pb (Stacey and Kramers 1975; Fig. 7a). The Cretaceous granitoids yield $^{206}Pb/^{204}Pb_i$ of 17.40 to 18.62, $^{207}Pb/^{204}Pb_i$ of 15.53 to 15.66, and $^{208}Pb/^{204}Pb_i$ of 38.47 to 39.85 (Tables 2 and 3; Fig. 7). Except for the relatively radiogenic samples from the Owlshead Mountains and Salt Spring Hills, the Cretaceous samples yield slightly smaller $^{207}Pb/^{204}Pb_i$ than predicted by the growth curve of average crustal Pb. On average, the Cretaceous samples yield larger $^{208}Pb/^{204}Pb_i$ than the Jurassic samples (Fig. 7b). The Cretaceous samples thus point to a greater relative Th/U (i.e. a more pronounced Mojave-type character) than the Jurassic samples. The Skidoo granodiorite has the greatest $^{208}Pb/^{204}Pb_i$ relative to $^{206}Pb/^{204}Pb_i$ of our samples.

Mafic rocks

The Jurassic and Cretaceous mafic samples have rather similar $^{147}Sm/^{144}Nd$, but measured $^{143}Nd/^{144}Nd$ and, thus, ϵ_{Ndi}, are different (Tables 2 and 3). The Jurassic quartz diorite dike yields an ϵ_{Ndi} of –8.0 whereas the Cretaceous gabbro has an ϵ_{Ndi} of –3.2 (the most radiogenic Nd isotopic composition of all the samples analyzed in this study). T_{DM} of the Jurassic and Cretaceous samples are 1.49 and 1.23 Ga, respectively. The two mafic samples have smaller $^{87}Rb/^{86}Sr$ and $^{87}Sr/^{86}Sr$ than most of the granitoids (Fig. 6b) and yield $^{87}Sr/^{86}Sr_i$ of 0.7093 (quartz diorite) and 0.7060 (gabbro); the gabbro thus shows the least radiogenic Sr isotopic composition of the samples analyzed in this study. The Pb isotopes of the two mafic rocks are rather similar to those of the granitoid rocks. The quartz diorite ($^{206}Pb/^{204}Pb_i = 18.10$, $^{207}Pb/^{204}Pb_i = 15.58$, $^{208}Pb/^{204}Pb_i = 39.24$) is more radiogenic than the gabbro ($^{206}Pb/^{204}Pb_i = 17.69$, $^{207}Pb/^{204}Pb_i = 15.54$, $^{208}Pb/^{204}Pb_i = 38.88$). Both plot within the field of the Mojave crustal province (Fig. 7). The Jurassic quartz diorite yields a larger $^{208}Pb/^{204}Pb_i$ than most of the Jurassic granitoids; the Cretaceous gabbro has a $^{208}Pb/^{204}Pb_i$ similar to the Cretaceous granitoids (Fig. 7b).

Discussion

Cordilleran granitoids are often used to model crustal provinces along the Mesozoic margin of North America. Variations in isotopic composition allow inferences regarding the age of the source rocks, mass budget of juvenile vs. recycled components, and crustal domains with different isotopic histories (see Kistler and Peterman 1973, 1978; DePaolo 1981a; Farmer and DePaolo 1983, 1984; Kistler et al. 1986; Barton 1990; DePaolo et al. 1991; Coleman et al. 1995; Sisson et al. 1996). Here we compare the isotopic composition of Jurassic and Cretaceous plutons of the southern Death Valley region to Mesozoic plutons in the Mojave Desert as well as the Sierra Nevada and Peninsular Ranges batholiths. This discussion is followed by models on the origin of Mesozoic plutonic rocks in the region. As many of the coarse-grained granitoids and the Creta-

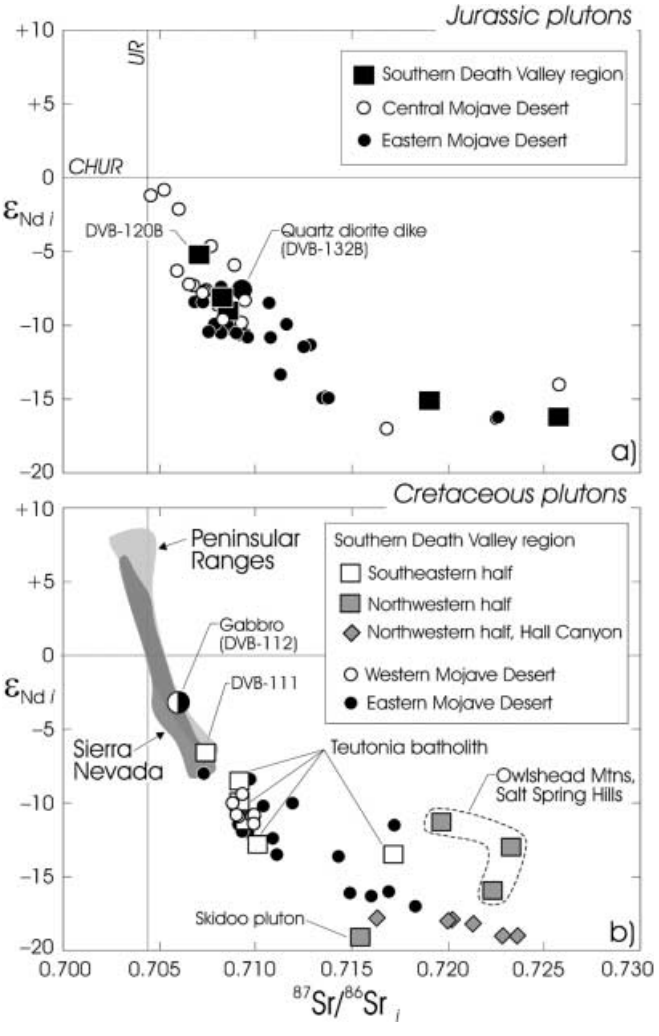

Fig. 8. ϵ_{Ndi} vs. $^{87}Sr/^{86}Sr_i$ diagrams comparing **a** Jurassic and **b** Cretaceous plutons of the southern Death Valley region to Mesozoic granitoids elsewhere in the Mojave Desert as well as Sierra Nevada and Peninsular Ranges batholiths. Jurassic reference data from Miller et al. (1990), Young et al. (1992), Miller and Wooden (1994), Gerber et al. (1995), and Miller and Glazner (1995); Cretaceous reference data from Kistler and Peterman (1973, 1978), DePaolo (1981a), Kistler et al. (1986), Miller and Wooden (1994), Allen et al. (1995), Barth et al. (1995), Gerber et al. (1995). Hall Canyon pluton data from Mahood et al. (1996). CHUR is Chondritic Uniform Reservoir and UR the Sr uniform mantle reservoir of DePaolo and Wasserburg (1976)

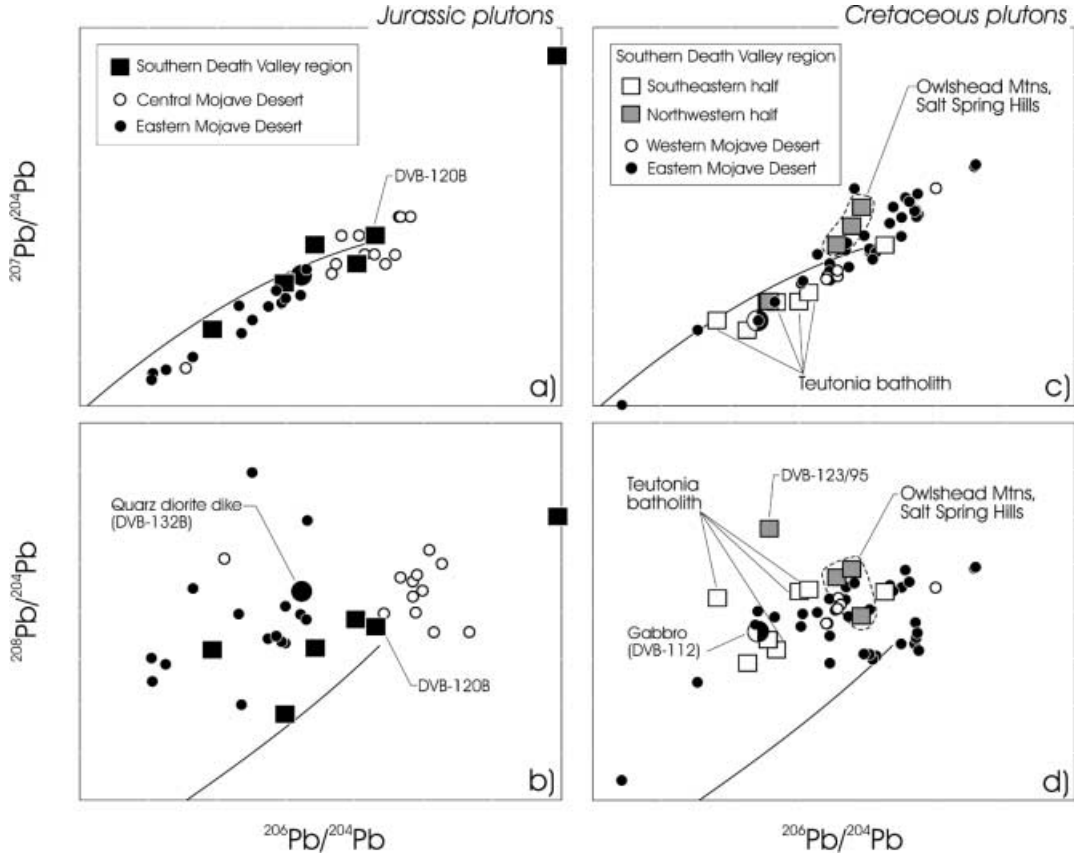

Fig. 9. $^{207}Pb/^{204}Pb$ vs. $^{206}Pb/^{204}Pb$ and $^{208}Pb/^{204}Pb$ vs. $^{206}Pb/^{204}Pb$ diagrams showing the initial Pb isotopic composition of the **a**, **b** Jurassic and **c**, **d** Cretaceous plutons of the southern Death Valley region compared with Jurassic and Cretaceous plutons in the eastern and west-central parts of the Mojave Desert. Data on eastern and central Mojave Desert are feldspar or age-corrected whole rock compositions, except Jurassic central Mojave Desert granitoids in **b**, which are represented by present-day whole rock values. Each diagram shows the growth curve for average crustal Pb (Stacey and Kramers 1975) for reference. Data for the plutons in the central and western Mojave Desert from Miller and Glazner (1995) and Barth et al. (1995), those in the eastern Mojave Desert from John and Wooden (1990), Miller et al. (1990), Karlstrom et al. (1993), Allen et al. (1995), and Gerber et al. (1995)

ceous gabbro are cumulate in nature, emphasis is laid on isotopic rather than elemental compositions.

Regional comparisons

The isotopic compositions of Jurassic and Cretaceous plutons within the southern Death Valley region are compared with Mesozoic granitoids from the Mojave Desert in Figs. 8 and 9. Although there is considerable overlap, Mesozoic granitoids from the central Mojave Desert are, on average, more juvenile (higher ϵ_{Ndi}, lower $^{87}Sr/^{86}Sr_i$) than plutons from the eastern Mojave Desert. Jurassic plutons from the southern Death Valley region show characteristics of both (Fig. 8a). Granodiorite in Sheep Canyon and Old Mormon Springs and the quartz diorite dike yield ϵ_{Ndi} and $^{87}Sr/^{86}Sr_i$ ratios that are intermediate to the range of ϵ_{Ndi} and $^{87}Sr/^{86}Sr_i$ of Jurassic plutons from the Mojave Desert. Monzogranite porphyry of Manly Peak, however, with ϵ_{Ndi} of –5.2 and $^{87}Sr/^{86}Sr_i$ of 0.7071, is our most juvenile granitoid sample and is similar isotopically to Jurassic granitoids from the central Mojave Desert (Fig. 8a). Jurassic granitoids in Warm Springs Canyon yield ϵ_{Ndi} of –15.1 and –16.2, and $^{87}Sr/^{86}Sr_i$ of 0.7191 and 0.7258 and are similar isotopically to ancient crust beneath the eastern Mojave Desert (Fig. 8a).

Cretaceous granitoids in the southeastern half of the southern Death Valley region yield ϵ_{Ndi} and $^{87}Sr/^{86}Sr_i$ ratios that plot within the range of Cretaceous plutons from the Mojave Desert (Fig. 8b). Cretaceous granitoids from the northwestern half of the southern Death Valley region yield, on average, lower ϵ_{Ndi} and higher $^{87}Sr/^{86}Sr_i$. Our most juvenile Cretaceous granitoid sample, the Rock Spring granodiorite, is from the southeastern half of the region and yields less radiogenic Nd and more radiogenic Sr than most of the Cretaceous granitoids in the Peninsular Ranges and Sierra Nevada batholiths (Fig. 8b). These batholiths are located west of the craton margin (Kistler and Peterman 1978) and were generated by mixing of mantle-derived magmas with relatively young (not cratonic) crust (e.g., DePaolo 1981a; Kistler et al. 1986; Coleman et al. 1995). The Skidoo granodiorite in the northwestern half of the region plots below the trend of Nd and Sr isotopic ratios from the Mojave Desert (Fig. 8b).

Jurassic and Cretaceous granitoids from the southern Death Valley region yield initial Pb isotopic ratios that

are, in general, similar to those from Mesozoic granitoids in the Mojave Desert (Fig. 9). Monzonite porphyry of Manly Peak and granodiorite from Old Mormon Springs yield Pb isotopic ratios that are similar to Jurassic granitoids from the central Mojave Desert; all the other Jurassic granitoids (except Warm Springs tonalite) and the quartz diorite dike, yield initial Pb isotopic ratios that are similar to those from the eastern Mojave Desert (Fig. 9a). Save for the Skidoo granite, Cretaceous granitoids from the northwestern half of the region yield higher $^{206}Pb/^{204}Pb_i$ and $^{207}Pb/^{204}Pb_i$ than granitoids from the southeastern half of the region (Fig. 9c).

The isotopic composition of the quartz diorite dike at Old Mormon Springs (ϵ_{Ndi} –8.1, $^{87}Sr/^{86}Sr_i$ 0.7093, $^{206}Pb/^{204}Pb_i$ 18.10) is similar to Jurassic diorite and gabbro plutons in the eastern Mojave Desert as well as Cenozoic basalts in eastern California and western Nevada. Jurassic diorites of the Bristol Lake region just south of southern Death Valley region yield ϵ_{Ndi} of –7.4 to –10.4 and $^{87}Sr/^{86}Sr_i$ of 0.7068 to 0.7085 (Young et al. 1992). Farther south, the Jurassic Ship Mountain intrusive suite includes gabbros and diorites with ϵ_{Ndi} between –8.4 and –10.8 and $^{87}Sr/^{86}Sr_i > 0.708$ (Gerber et al. 1995). An ancient enriched mantle lithosphere was invoked as the source of these mafic rocks by these authors. Farmer et al. (1989) reported that extension-related Tertiary and Quaternary basalts in eastern California and adjacent Nevada (north of the southern Death Valley region) yield $\epsilon_{Nd} < -8$, $^{87}Sr/^{86}Sr_i > 0.707$, and $^{206}Pb/^{204}Pb$ 17.8–18.8. They concluded that these basalts were derived from Precambrian enriched mantle lithosphere that had been preserved because this part of the Cordilleran interior had remained an amagmatic zone since the end of the Precambrian. The isotopic composition and chemical signature of the Old Mormon Springs quartz diorite dike, combined with regional isotopic data, suggest that an enriched mantle lithosphere was present beneath the central southern Death Valley region during the Jurassic.

The 93-Ma Black Canyon gabbro on the southeastern flank of the southern Death Valley region is clearly more juvenile (ϵ_{Ndi} of –3.2, $^{87}Sr/^{86}Sr_i$ 0.7060) than the quartz diorite dike at Old Mormon Springs (ϵ_{Ndi} of –8.0, $^{87}Sr/^{86}Sr_i$ 0.7093). Chemically, the gabbro is relatively evolved (mg# 61; Table 4) and may not represent the Nd and Sr isotopic composition of its mantle source. It does, however, yield a lower limit for the ϵ_{Ndi} and upper limit for the $^{87}Sr/^{86}Sr_i$ of the mantle source. The gabbro may reflect hybridization of the crust by juvenile mantle-derived melts in the southeastern part of the southern Death Valley region in Late Cretaceous time (see also Miller and Wooden 1994).

Origin of Mesozoic plutonic rocks in the southern Death Valley region

To examine the origin of the Jurassic and Cretaceous granitoids of the southern Death Valley region, an estimate of possible end member compositions and their variation through time is required. These include the character of the Mesozoic subcontinental mantle and composition of crustal domains involved in Mesozoic magmatism. Farmer et al. (1989), Young et al. (1992), Gerber et al. (1995), and Miller and Glazner (1995) concluded that asthenospheric mantle (high ϵ_{Ndi} and $^{206}Pb/^{204}Pb_i$, low $^{87}Sr/^{86}Sr_i$) was involved in the generation of Jurassic plutons in the central Mojave Desert, whereas lithospheric mantle (low ϵ_{Ndi} and $^{206}Pb/^{204}Pb_i$, high $^{87}Sr/^{86}Sr_i$) probably underlies the eastern part of the desert.

Our recent work on the cratonic rocks of the southern Death Valley region (Rämö and Calzia 1998) has shown that the Proterozoic crust in this part of the Mojave Desert has an older overall signature (T_{DM} up to 2.6 Ga) than previously anticipated (Bennett and DePaolo 1987). These cratonic rocks, or their lower crustal equivalents, have obviously contributed to the Mesozoic plutons of the region (Wooden et al. 1988) and are responsible for the very low ϵ_{Ndi} and high $^{87}Sr/^{86}Sr_i$ of some of them. Mantle melts generated during Mesozoic subduction probably had a profound influence on the overall composition of the Mojave crust, resulting in hybrid crustal domains with a less-cratonic character (Miller and Wooden 1994). Mesozoic hybrid crust thus represents another viable source, at least for the Cretaceous plutons of our study area.

Most of the Jurassic granitoids of the southern Death Valley region consist of relatively mafic, calc-alkaline plutons with consistent trends for many of the major and trace elements (Fig. 3). They show, however, quite variable initial isotopic compositions (ϵ_{Ndi} –5.2 to –16.2, $^{87}Sr/^{86}Sr_i$ 0.7071 to 0.7258, and $^{206}Pb/^{204}Pb_i$ 17.46–19.97). The unradiogenic Nd and radiogenic Sr in some samples invoke Precambrian crust as a distinct component of the melt, whereas the relatively juvenile composition of other samples shows that a substantial mantle component was probably also involved. As the isotopic compositions of the granitoids vary at random relative to elemental geochemical variables (Fig. 10), a single process of mantle-derived melt fractionating and assimilating ancient crustal material is not viable. The isotopic variations can be explained, however, by mixing of mantle melts with partial melts of distinct crustal materials.

To explore the mixing hypothesis further, we constructed mixing paths for two mantle end members and three model crustal assimilants (Fig. 11). A depleted asthenospheric mantle source (ϵ_{Ndi} +4, $^{87}Sr/^{86}Sr_i$ 0.7035; Table 4) mixed with the mean of Mesozoic intrusive rocks of the Mojave Desert (ϵ_{Ndi} –11.7, $^{87}Sr/^{86}Sr_i$ 0.711; Miller and Wooden 1994) yields a mixing hyperbola that is compatible with our three most juvenile Jurassic granitoids (monzogranite of Manly Peak and granodiorites in Sheep Canyon and Old Mormon Springs), but fails to take into account the low ϵ_{Ndi}, high $^{87}Sr/^{86}Sr_i$ samples (granodiorite

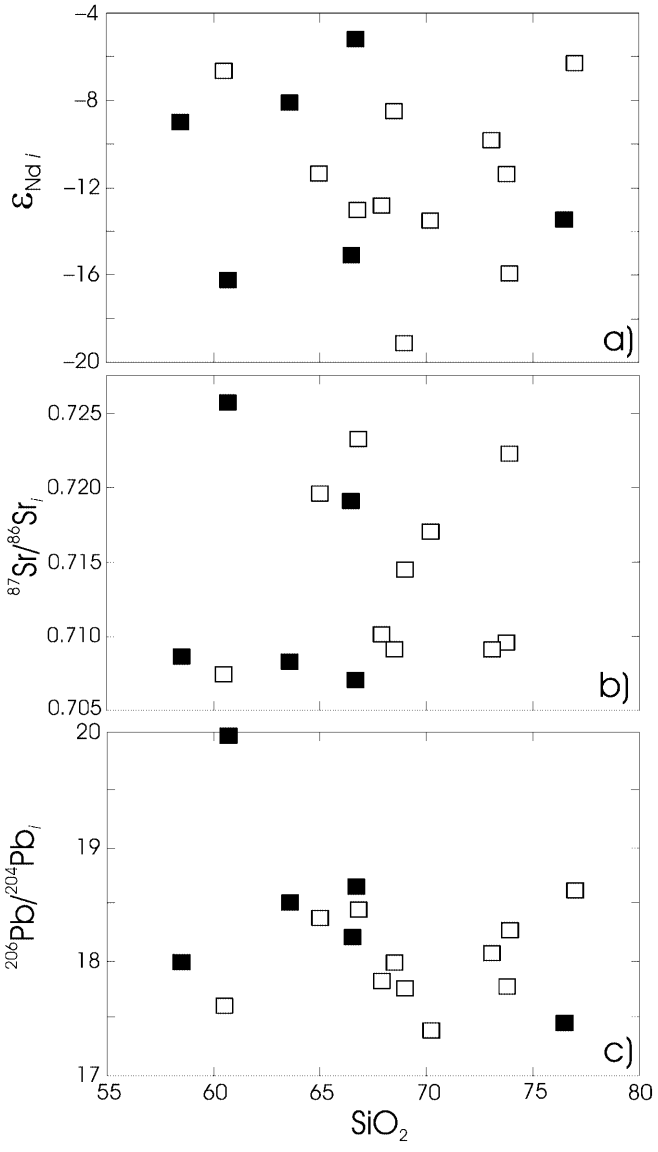

Fig. 10. Composition of the Jurassic (*black squares*) and Cretaceous (*open squares*) granitoids of the southern Death Valley region shown in **a** ϵ_{Ndi} vs. SiO_2, **b** $^{87}Sr/^{86}Sr_i$ vs. SiO_2, and **c** $^{206}Pb/^{204}Pb_i$ vs. SiO_2 diagrams. SiO_2 is expressed in wt%. Note that two high-silica samples (DVB-109, DVB-131) plot off the diagram in **b**

porphyry and tonalite in Warm Springs Canyon; Fig. 11a). Substituting mean Proterozoic crust of Miller and Wooden (1994; ϵ_{Ndi} –17.9, $^{87}Sr/^{86}Sr_i$ 0.739) as the crustal end member results in a hyperbola that runs through these two samples; the Warm Springs tonalite represents an almost pure anatectic melt of mean Proterozoic crust. If an enriched lithospheric mantle source (ϵ_{Ndi} –6, $^{87}Sr/^{86}Sr_i$ 0.707; Table 4) is used as the mafic end member, the mixing paths are rather similar to those using a depleted asthenospheric mantle source (Fig. 11b). The enriched mantle – mean Proterozoic crust mixing model, however, does not yield as perfect a fit as the depleted mantle model; the monzogranite porphyry of Manly Peak, for example, is slightly more juvenile than the mantle end member. Overall, our data suggest that Jurassic plutonic rocks in the southern Death Valley region were derived by mixing of mantle melts with Proterozoic crust.

With one clear exception (Rock Spring granodiorite), Cretaceous granitoids of the southern Death Valley region are more silicic (Fig. 4), poorer in plagioclase component (Fig. 2), and yield, on average, slightly more unradiogenic Nd, more radiogenic Sr, and more thorogenic Pb (Figs. 7 and 11) than the Jurassic granitoids. Most of the Cretaceous granitoids plot on mixing hyperbolas between enriched lithospheric mantle and mean Proterozoic crust or the mean composition of the cratonic rocks of the southern Death Valley region. The Rock Spring granodiorite, however, cannot be modeled with lithospheric mantle as the mafic end member because the granodiorite would represent an almost pure mantle melt (Fig. 11b); it could have derived, however, from a crustally contaminated melt that originated from a less-enriched lithospheric mantle. Quartz monzonite and the granodiorite dike from the Owlshead Mountains yield higher $^{87}Sr/^{86}Sr_i$ than the other Cretaceous samples with comparable ϵ_{Ndi} and plot on a mixing hyperbola with cratonic rocks of the southern Death Valley region as the crustal end member (Fig. 11). Combined, these data suggest that the Cretaceous magmatic history varies across the southern Death Valley region. The heterogeneous composition of the Cretaceous plutons is probably related to the different age and character of crustal source rocks (including Jurassic assimilates) in the southeastern and northwestern halves of the region. Given the age of the granitoid plutons, however, these magmatic events were synchronous across the southern Death Valley region.

The Kessler Springs monzogranite and Skidoo granodiorite yield lower ϵ_{Ndi} relative to $^{87}Sr/^{86}Sr_i$ than the remainder of the Cretaceous plutons of the region. These samples would plot on a mixing hyperbola between a mantle end member and Proterozoic crust with relatively low $^{87}Sr/^{86}Sr_i$ (Fig. 11b). The Skidoo granodiorite also yields the most thorogenic Pb isotopic composition and the most pronounced Mojave-type signature of all our Cretaceous granites (Fig. 7). The Hall Canyon pluton, located approximately 20 km south of the Skidoo pluton, yields similar Nd, but more radiogenic Sr isotopic compositions than the Skidoo granodiorite (Mahood et al. 1996; Fig. 11b). Mahood et al. concluded that the Hall Canyon pluton was derived from an entirely crustal source.

According to Hanchar et al. (1994), quartzo-feldspathic, aluminous, and quartzitic xenoliths collected from Tertiary dikes in the eastern Mojave Desert yield ϵ_{Nd} (at 95 Ma) from –21 to –18, and $^{87}Sr/^{86}Sr_i$ from 0.710 to 0.755. They concluded that the xenoliths were Precambrian in origin, but were subjected to a melting event during the Phanerozoic (possibly during Mesozoic arc magmatism). Figure 11b shows that the Nd and Sr isotopic composition of most of these quartzo-felds-

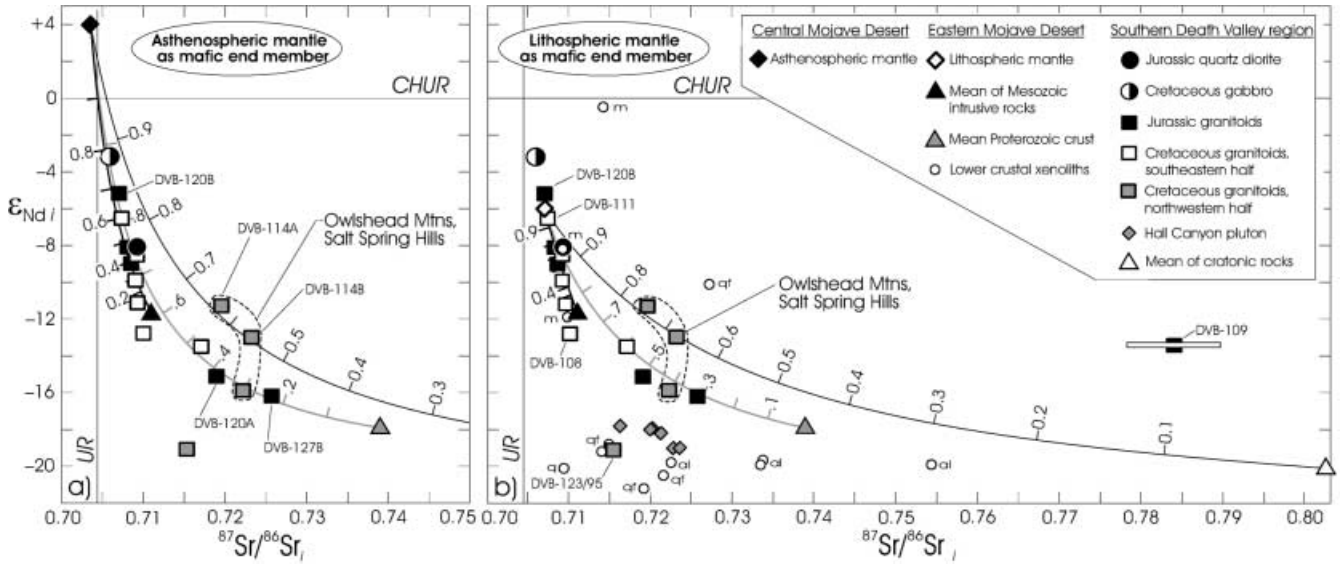

Fig. 11. ϵ_{Ndi} vs. $^{87}Sr/^{86}Sr_i$ diagrams showing granitoids from the southern Death Valley region and mixing hyperbolas between three crustal end members and **a** a slightly depleted (asthenospheric) mantle and **b** a slightly enriched (lithospheric) mantle. In **b** the composition of the Ivanpah Mountain monzogranite DVB-109 with anomalous, rather inaccurate $^{87}Sr/^{86}Sr_i$ is also shown (*white error bar*; the error of the calculated $^{87}Sr/^{86}Sr_i$ for the other samples is less than the *symbol size*; see Tables 2 and 3). Data for the Jurassic quartz diorite dike, Cretaceous gabbro, and Hall Canyon pluton (Mahood et al. 1996) are also shown, as are compositions of quartzose (*q*), quartzo-feldspathic (*qf*), aluminous (*al*), and mafic (*m*) crustal xenoliths from the eastern Mojave Desert (calculated at 95 Ma; Hanchar et al. 1994). Mean composition for the cratonic rocks of the southern Death Valley region (ϵ_{Ndi} –20.1, $^{87}Sr/^{86}Sr_i$ 0.8029) is based on Rämö and Calzia (1998) and unpublished data by the authors. *Tick marks* indicate fraction of mafic end member in each mixture. For details on end member compositions, see text and Table 4. CHUR and UR as in Fig. 8

pathic xenoliths is similar to that of the Skidoo and Hall Canyon plutons and may approach the composition of the crustal source rocks of these plutons (or unmelted residue left behind during anatexis). The composition of the aluminous xenoliths extends from the field defined by the quartzo-feldspathic xenoliths toward the mean composition of cratonic rocks of the southern Death Valley region (Fig. 11b). These cratonic rocks include a major (and variable) Archean source component that was probably introduced as sedimentary material in a convergent margin setting (Rämö and Calzia 1998). Our data, combined with Hanchar et al. (1994) data, suggest that the Skidoo granodiorite was derived by anatexis of cratonic crust.

Crustal domains

Chemical and isotopic data suggest that at least two different crustal domains existed during Mesozoic magmatism in the southern Death Valley region. Jurassic granitoids in the northwestern half of this region (domain 1 in Fig. 12) yield ϵ_{Ndi} from –8.1 to –16.2 and $^{87}Sr/^{86}Sr_i$ from 0.708 to 0.726; Cretaceous granitoids within the same domain yield ϵ_{Ndi} from –11.3 to –19.1 and $^{87}Sr/^{86}Sr_i$ from 0.714 to 0.723. Cretaceous granitoids in the southeastern half of this region (domain 2 in Fig. 12) yield ϵ_{Ndi} from –6.3 to –13.5 and $^{87}Sr/^{86}Sr_i$ from 0.707 to 0.717. These data suggest that the northwestern half of the region is underlain by isotopically more evolved (and older) Proterozoic cratonic rocks. Nd isotopic data on cratonic rocks of this region (Rämö and Calzia 1998) suggest that cratonic rocks in domain 1 contain a larger Archean component than those in domain 2. The isotopic evidence for a less enriched mantle beneath domain 2 suggests that this area was invaded by relatively juvenile magmas at ~97–93 Ma. The tectonic significance of these juvenile magmas is not known.

The origin of the Late Jurassic monzonite porphyry of Manly Peak on the western flank of domain 1 in the southwestern Panamint Range (Fig. 1) is enigmatic. The isotopic composition of the monzonite porphyry is similar to Jurassic plutonic rocks that intrude eugeoclinal rocks in the central Mojave Desert (domain 3 of Fig. 12; Miller and Glazner 1995). Eugeoclinal rocks in the southern Panamint Range include the Triassic Butte Valley and Warm Springs formations as well as Triassic metavolcanic rocks (Wrucke 1966; Cole and Marzolf 1986). Perhaps the relatively juvenile isotopic composition of the monzonite porphyry was caused by assimilation of eugeoclinal rocks in the southern Panamint Range. Granodiorite porphyry and tonalite in Warm Springs Canyon (~10 km east of the monzogranite porphyry), however, intrude the same eugeoclinal rocks as the monzonite porphyry, but yield Nd, Sr, and Pb isotopic ratios that are similar to Proterozoic crust in domain 1 (see also Fig. 1). These data suggest that an isotopic boundary exists between the plutons in Warm Springs Canyon and the monzonite porphyry of Manly Peak; this boundary may delineate the western edge of Proterozoic crust (the craton) during the Jurassic (Fig. 12). On the other hand, the monzonite porphyry of

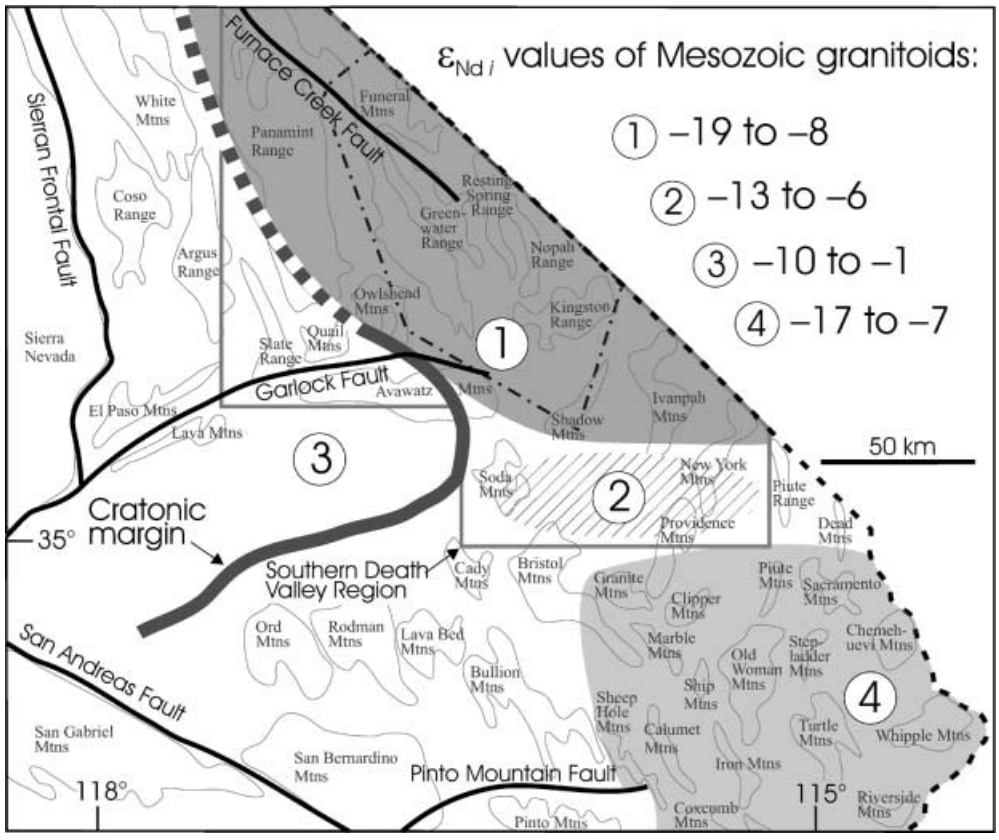

Fig. 12. Sketch map of southeastern California showing crustal domains in the Mojave Desert and vicinity as defined by ϵ_{Ndi} values of Mesozoic granitoid plutons. Our data for the plutons in the southern Death Valley region reveal a juvenile domain in easternmost California at approximately 35°N latitude. This domain (number 2) separates two other cratonal blocks (1 and 4) that have less radiogenic and slightly different Nd isotopic signatures. Cratonic margin in the central Mojave Desert is the inferred miogeocline–cratonal hingeline from Martin and Walker (1992) which, according to our data, probably continues northwestward along the western margin of the Panamint Range. Major faults and the southwestern part of the amagmatic zone of Farmer et al. (1989; *dot-dashed*) are also shown. Nd data from this study and references mentioned in Fig. 8

Manly Peak cuts the Big Horn Canyon Fault (McKenna et al. 1993) and is cut by left-lateral faults related to Late Cretaceous crustal extension in the Panamint Range (Andrew 2000). The Big Horn Canyon Fault places younger rocks over older rocks and is correlated with the Harrisburg Fault, an extensional fault in the northern Panamint Range. These data suggest that the monzonite porphyry is synchronous with pre-Late Jurassic to Late Cretaceous crustal extension in the Panamint Range. Calzia (1990) concluded that mid-Tertiary granitic magmas that are syn-extensional in the southern Death Valley region are derived by partial melting of crustal rocks by mantle-derived mafic magmas. Perhaps the monzonite porphyry of Manly Peak is a Late Jurassic example of the mid-Tertiary relation between coeval magmatism and crustal extension in the southern Death Valley region.

The origin and significance of domain 2 is also puzzling. Cretaceous granitoids in this domain yield Nd isotopic ratios that are more juvenile than those of the Cretaceous granitoids in domain 1 (the northwestern half of the southern Death Valley region) and domain 4 (the eastern Mojave Desert). Eugeoclinal rocks are present in the Soda Mountains (Grose 1959; Walker and Wardlaw 1989) and southern Clark Mountains (Evans 1971) along the west and east sides, respectively, of domain 2 (Fig. 12). It is possible that the eugeoclinal rocks were involved in the 97-Ma magmatism in domain 2, but had been eroded prior to the 95-Ma magmatism in domain 1; erosion may have been related to Late Jurassic–Late Cretaceous crustal extension in the Panamint Mountains (McKenna et al. 1993; Andrew 2000). On the other hand, the anomalously juvenile character of the Black Canyon gabbro in domain 2 requires a juvenile mantle source beneath the southeastern part of the southern Death Valley region prior to 93 Ma. This would be consistent with Late Jurassic or Early Cretaceous hybridization of the crust with juvenile mantle melts. In any event, our data suggest that domain 2 delineates a crustal boundary between two distinct cratonic domains (1 and 4, Fig. 12) in the southern Death Valley region and the eastern Mojave Desert. The cratonic domain in the north (northwestern half of the southern Death Valley region) has a slightly more ancient character.

Conclusions

1. Jurassic and Cretaceous granitoid plutons in the southern Death Valley region of southeastern California show differences in their petrographic and geochemical composition. The former are, in general, mafic biotite–hornblende granodiorites (or, occasionally, monzogranite, quartz monzonite, and tonalite) whereas the latter are more heterogeneous and silicic (in general, monzogranites), including marginally peraluminous rock types.

2. The Nd, Sr, and Pb isotopic composition of the Jurassic and Cretaceous plutons varies widely and can be modeled as the result of mixing of mantle-derived and crust-derived magmas. Contribution from pre-existing crust is more evident in the Cretaceous plutons; some of the peraluminous granitoids were presumably generated by intracrustal anatexis.
3. Contrasting isotopic composition of Jurassic granitoids in the southern Panamint Range suggests that the craton margin that runs across the west-central Mojave Desert continues northwestward to the western flank of the Panamint Range.
4. Initial isotopic composition of Cretaceous plutons in the southern Death Valley region reveal an unusually juvenile lithospheric block at approximately 35°N latitude. The block may reflect Cretaceous invasion of crust by juvenile mantle melts. It also separates two Precambrian crustal terrains of slightly different overall composition and age, the terrane in the northwestern half of the southern Death Valley region having a more ancient character.

Acknowledgements O.T.R. acknowledges the staff of the Unit for Isotope Geology, Geological Survey of Finland, for help while performing the isotopic analyses. Comments from Calvin Miller and an anonymous reviewer led to substantial improvement of the paper. Bennie Troxel is thanked for providing field accommodation in Shoshone. We were also absolutely thrilled about the pleasures of the Tecopa Hot Springs during the field sessions. O.T.R. and P.J.K. were funded by the Academy of Finland (Project 36002).

Appendix

Jurassic plutons

- DVB-109. Ivanpah monzogranite, Ivanpah Mountains. White, medium-grained, equigranular massive leucomonzogranite composed essentially of alkali feldspar (35 vol%), albite (33%; $An_{5–10}$), and quartz (31%). Accessory minerals include biotite, oxide, rutile, and fluorite; secondary muscovite is present. Plagioclase is strongly altered and turbid; water-clear albite rims are present between plagioclase and alkali feldspar grains.
- DVB-116. Biotite–hornblende granodiorite, Sheep Canyon, eastern Avawatz Mountains. Slightly schistose, medium- to coarse-grained, gray melagranodiorite with microcline phenocrysts up to 10 mm in diameter. Biotite and hornblende are found as poikilitic grains, 10–15 mm in diameter, enclosing euhedral crystals of epidote and titanite. The main silicates are oligoclase (34%), quartz (18%), alkali feldspar (17%), hornblende (15%), and biotite (11%). In addition to epidote (3%) and titanite ($< 1\%$), accessory minerals comprise apatite, chlorite, zircon, oxide, and sericite.
- DVB-120A. Granodiorite porphyry, Warm Springs Canyon, southeastern Panamint Range. Light gray, porphyritic (glomerophyric) granodiorite porphyry. The phenocryst assemblage comprises plagioclase (74%), dark mica (15%), and hornblende (7%) as well as microphenocrysts of oxide (3%) and quartz (2%). The plagioclase phenocrysts are strongly zoned ($\sim An_{25–45}$) and up to 10 mm in maximum dimension. The groundmass is fine grained, granular, and consists mainly of alkali feldspar and quartz. Accessory zircon and apatite are also present.
- DVB-120B. Monzogranite porphyry of Manly Peak, Goler Wash, southern Panamint Range. Light brownish gray, fine to medium-grained monzogranite porphyry with phenocrysts of plagioclase (77% of the phenocryst assemblage; maximum dimension 5 mm), biotite (8%; maximum dimension 2 mm), amphibole (7%; maximum dimension 2 mm; completely altered), and microphenocrysts of quartz (7%) and oxide (1%) set in an aphanitic granitic groundmass. The phenocrysts define a distinct magmatic foliation; oligoclase crystals give the rock a glomerophyric appearance and are partly replaced by carbonate.
- DVB-127B. Biotite tonalite, Warm Springs Canyon, southeastern Panamint Range. Gray, medium- and even-grained, massive biotite tonalite. The main minerals are oligoclase (52%), quartz (29%), biotite (12%), and alkali feldspar (5%). Quartz and alkali feldspar are found in the interstices of plagioclase grains that, in general, are subhedral and strongly zoned. The average grain size is $\sim$3 mm; fine-grained mafic enclaves are common. Accessory minerals are hornblende (1%), oxide, zircon, titanite, and epidote as well as secondary carbonate and chlorite.
- DVB-132A. Hornblende–biotite granodiorite, Old Mormon Springs, eastern Avawatz Mountains. Medium-grained, slightly schistose gray hornblende-biotite melagranodiorite. Resembles DVB-116, but is fine-grained and not porphyritic. The main minerals are oligoclase (37%), quartz (19%), biotite (14%), hornblende (13%), and alkali feldspar (12%). Biotite and hornblende are found as poikilitic grains that enclose euhedral epidote (3%; 1.2 mm in maximum dimension) and titanite crystals. Further accessory minerals include zircon, oxide, and apatite.
- DVB-132B. Biotite–hornblende quartz diorite, Old Mormon Springs, eastern Avawatz Mountains. Approximately 1-m-wide dike cutting sample DVB-132A. The dike is dark gray, medium- and even-grained (average grain size 1–2 mm), and massive with no discernable fabric. Main minerals are plagioclase (44%; An_{40}), hornblende (27%), biotite (16%), and quartz (8%). Epidote, titanite, apatite, oxide, and alkali feldspar are present in minor amounts.

Cretaceous plutons

- DVB-107. Biotite monzogranite, Halloran Hills. Pinkish gray medium- to coarse-grained, equigranular biotite monzogranite with no clear fabric. The average grain size is 5 mm; some alkali feldspar crystals with a

maximum dimension of 10 mm are also present. The main minerals are oligoclase (37%), alkali feldspar (31%), quartz (22%), and biotite (10%). Accessory minerals include oxide, titanite, apatite, zircon, and secondary carbonate.

- DVB-108. Kessler Springs biotite monzogranite, Ivanpah Mountains. Pale gray medium- to coarse-grained biotite monzogranite with occasional pink alkali feldspar phenocrysts up to 2 cm in maximum dimension. The average grain size is ~5 mm and no fabric is present. Main minerals are oligoclase (34%), alkali feldspar (34%), quartz (22%), and biotite (8%). Plagioclase crystals are strongly zoned; biotite forms subhedral, relatively small (1–2 mm in maximum diameter) crystals. Accessory minerals are oxide, green amphibole, titanite, apatite, zircon, and secondary carbonate and chlorite.
- DVB-110. Quartz alkali feldspar syenite, Teutonia Peak. Pale gray, coarse-grained, leucocratic quartz alkali feldspar syenite. Alkali feldspar (85%) occurs as <3.5-cm-long megacrysts set in a matrix of granular quartz (11%), alkali feldspar, and rare oligoclase. Subhedral amphibole and intensively altered biotite are present in minor amounts, as are oxide, apatite, and zircon.
- DVB-111. Rock Spring hornblende-biotite granodiorite, central Providence Mountains. Medium to coarse-grained, dark gray melagranodiorite with oligoclase microphenocrysts up to 7 mm in maximum dimension. The rock shows a strong fabric with aligned arrays of biotite and hornblende and is somewhat cataclastic with recrystallized quartz filling the interstices of oligoclase grains. Main minerals are oligoclase (43%), quartz (15%), biotite (15%), hornblende (13%), and alkali feldspar (11%). Accessory augite (1%) is found in the cores of hornblende grains; accessory phases also include titanite, oxide, apatite, zircon, and epidote.
- DVB-112. Black Canyon biotite–hornblende gabbro, central Providence Mountains. Dark, medium-grained, equigranular biotite hornblende gabbro that is heterogeneous with abundant mafic enclaves. Average grain size is ~2 mm and the rock consists of hornblende (44%), plagioclase (41%; $An_{55–60}$), and biotite (11%). Plagioclase is subhedral and partly replaced by white mica. Hornblende (unaltered) and biotite (partly replaced by chlorite and epidote) are anhedral relative to plagioclase. Accessory minerals include oxide (3%), apatite, and alkali feldspar.
- DVB-113. Mid Hills biotite monzogranite, central Providence Mountains. White, medium-grained, equigranular biotite leucomonzogranite. Primary minerals are oligoclase (43%), quartz (29%), and alkali feldspar (25%). Biotite (3%) is found as ~1-mm-long subhedral grains. Other accessory minerals are titanite, oxide, white mica, and zircon.
- DVB-114A. Biotite–hornblende quartz monzonite, Owlshead Mountains. Pale brown, medium-grained, equigranular biotite–hornblende leucoquartz monzonite. Primary minerals are microcline (43%), oligoclase (31%), and quartz (16%). Hornblende (5%) and biotite (4%) form clusters that define a faint lineation. The rock also contains minor amounts of oxide, zircon, apatite, titanite, and secondary white mica (the latter replacing plagioclase).
- DVB-114B. Hornblende–biotite granodiorite, Owlshead Mountains. Gray, medium-grained, equigranular hornblende–biotite granodiorite dike cutting sample DVB-114A. Primary minerals are plagioclase (39%), quartz (31%), biotite (15%), and alkali feldspar (11%). Plagioclase is found as strongly zoned ($An_{25–40}$) subhedral grains up to 4 mm in maximum dimension. Accessory phases are hornblende (2%), oxide, apatite, titanite, zircon, allanite, and secondary chlorite, white mica, and epidote. The rock also contains mafic microgranular enclaves with abundant hornblende, biotite, and epidote.
- DVB-117. Biotite granite, Salt Spring Hills. Grayish pink, medium- to coarse-grained, massive biotite leucogranite with quartz (35%), oligoclase (32%), and perthite (29%). Euhedral oligoclase is strongly zoned, partly replaced by white mica and saussurite. Rare perthite microphenocrysts are present. Biotite (4%) is subhedral and occurs as 2- to 5-mm-long platy grains. Other accessory minerals include oxide, zircon, apatite, and secondary chlorite and white mica.
- DVB-123/95. Skidoo granodiorite, northern Panamint Range. Gray, strongly sheared, medium- to coarse-grained, sparsely porphyritic muscovite–biotite granodiorite. The rock consists of quartz (47%), oligoclase to (32%), and alkali feldspar (10%) in a granodiorite matrix with occasional alkali feldspar phenocrysts up to 1.5 cm long. Partly chloritized and epidotized biotite (6%) and muscovite (5%) are the main mafic minerals. Oligoclase is turbid and partially replaced by white mica and epidote.
- DVB-129. Hornblende–biotite monzogranite, southwest side of Cima Dome. Pale brown, coarse-grained, massive leucomonzogranite with alkali feldspar grains up to 1.5 cm long. Rock comprised of strongly zoned oligoclase (39%), quartz (30%), and alkali feldspar (23%). Fresh biotite (5%) and pale green amphibole (1.5%) are found as 1- to 3-mm-long grains. Additional accessory minerals include oxide, titanite, apatite, zircon, and secondary white mica and epidote.
- DVB-131. Zzyzx biotite alkali feldspar granite, Soda Mountains. Pale gray, medium- to coarse-grained, leucocratic alkali feldspar granite composed of mesoperthite (61%) and quartz (35%). Minor constituents are intergranular albite (2%), biotite (0.5%), oxide, and titanite.

References

Allen CM, Wooden JL, Howard KA, Foster DA, Tosdal RM (1995) Sources of the Early Cretaceous plutons in the Turtle and West Riverside Mountains, California: anomalous Cordilleran interior intrusions. J Petrol 36:1675–1700

Andrew J (2000) Late Cretaceous extension in the Panamint Range, California: implications for Tertiary Death Valley extension. Geol Soc Am Abstr Program 32:A-168

Applegate JDR, Walker JD, Hodges KV (1992) Late Cretaceous extensional unroofing in the Funeral Mountains metamorphic core complex, California. Geology 20:519–522

Armstrong RL, Suppe J (1973) Potassium–argon geochronometry of Mesozoic igneous rocks in Nevada, Utah, and southern California. Geol Soc Am Bull 84:1375–1392

Barth AP, Wooden JL, Tosdal RM, Morrison J (1995) Crustal contamination in the petrogenesis of a calc-alkalic rock series: Josephine Mountain intrusion, California. Geol Soc Am Bull 107:201–212

Barton MD (1990) Cretaceous magmatism, metamorphism, and metallogeny in the east-central Great Basin. In: Anderson JL (ed) The nature and origin of Cordilleran magmatism. Geol Soc Am Mem 174:283–302

Beckerman GM, Robinson JP, Anderson JL (1982) The Teutonia batholith: a large intrusive complex of Jurassic and Cretaceous age in the eastern Mojave Desert, California. In: Frost EG, Martin DL (eds) Mesozoic–Cenozoic tectonic evolution of the Colorado River region, California, Arizona, and Nevada. Geol Soc Am Field Trip Guidebook, pp 205–220

Bennett VC, DePaolo DJ (1987) Proterozoic crustal history of the western United States as determined by neodymium isotopic mapping. Geol Soc Am Bull 99:674–685

Boynton WV (1984) Cosmochemistry of the rare earth elements: meteorite studies. In: Henderson P (ed) Rare earth element geochemistry: developments in geochemistry, vol 2. Elsevier, Amsterdam, pp 63–114

Calzia JP (1990) Geologic studies in the Kingston Range, southern Death Valley, California. PhD Thesis, University of California, Davis

Calzia JP, Rämö OT (2000) Late Cenozoic crustal extension and magmatism, southern Death Valley region, California. In: Lageson DR, Peters SG, Lahren MM (eds) Great Basin and Sierra Nevada. Geol Soc Am Field Guide, vol 2, pp 135–164

Cole RD, Marzolf JE (1986) The transition from shallow water sedimentation to orogenic arc volcanism: the Triassic Butte Valley and Warm Springs Formations, southern Panamint Range – another piece of the puzzle. Geol Soc Am Abstr Program 18:96

Coleman DS, Glazner AF, Miller JS, Bradford KJ, Frost TP, Joye JL, Bachl CA (1995) Exposure of a Late Cretaceous layered mafic-felsic magma system in the central Sierra Nevada batholith, California. Contrib Mineral Petrol 120:129–136

DePaolo DJ (1981a) A neodymium and strontium isotopic study of the Mesozoic calc-alkaline granitic batholiths of the Sierra Nevada and Peninsular Ranges, California. J Geophys Res 86(B11):10470–10488

DePaolo DJ (1981b) Neodymium isotopes in the Colorado Front Range and crust-mantle evolution in the Proterozoic. Nature 291:193–196

DePaolo DJ, Wasserburg GJ (1976) Nd isotopic variations and petrogenetic models. Geophys Res Lett 3:249–252

DePaolo DJ, Linn AM, Schubert G (1991) The continental crustal age distribution: methods of determining mantle separation ages from Sm–Nd isotopic data and application to the southwestern United States. J Geophys Res 96(B2):2071–2088

DeWitt E, Armstrong RL, Sutter JF, Zartman RE (1984) U–Th–Pb, Rb–Sr, and Ar–Ar mineral and whole-rock isotopic systematics in a metamorphosed granitic terrane, southeastern California. Geol Soc Am Bull 95:723–739

Elliott BA (1999) Colour masks in digital image analysis: a technique for modal analyses of quartz saturated plutonic rocks. Bull Geol Soc Finland 71:233–241

Evans JR (1971) Geology and mineral deposits of the Mescal Range Quadrangle, San Bernardino, California. Calif Div Mines Geol Map Sheet 17

Farmer GL, DePaolo DJ (1983) Origin of Mesozoic and Tertiary granite in the western US and implications for pre-Mesozoic crustal structure. 1. Nd and Sr isotopic studies in the geocline of the northern Great Basin. J Geophys Res 88(B4):3379–3401

Farmer GL, DePaolo DJ (1984) Origin of Mesozoic and Tertiary granite in the western United States and implications for pre-Mesozoic crustal structure. 2. Nd and Sr isotopic studies of unmineralized and Cu- and Mo-mineralized granite in the Precambrian craton. J Geophys Res 89(B12):10141–10160

Farmer GL, Perry FV, Semken S, Crowe B, Curtis D, DePaolo DJ (1989) Isotopic evidence on the structure and origin of subcontinental lithospheric mantle in southern Nevada. J Geophys Res 94(B6):7885–7898

Fox LK, Miller DM (1990) Jurassic granitoids and related rocks of the southern Bristol Mountains, southern Providence Mountains, and Colton Hills, Mojave Desert, California. In: Anderson JL (ed) The nature and origin of Cordilleran magmatism. Geol Soc Am Mem 174:111–132

Gerber ME, Miller CF, Wooden JL (1995) Plutonism at the interior margin of the Jurassic magmatic arc, Mojave Desert, California. In: Miller DM, Busby C (eds) Jurassic magmatism and tectonics of the North American Cordillera. Geol Soc Am Spec Pap 299:351–374

Grose LT (1959) Structure and petrology of the northeast part of the Soda Mountains, San Bernardino County, California. Geol Soc Am Bull 70:1509–1547

Gulson BL, Mizon KJ (1979) Lead isotopes as a tool for gossan assessment in base metal exploration. J Geochem Explor 11:299–320

Gulson BL, Korsch MJ, Cameron M, Vaasjoki M, Mizon KJ, Porritt PM, Carr GR, Kamper C, Dean JA, Calvez J-Y (1984) Lead isotope ratio measurements using the Isomass 54E in fully automatic mode. Int J Mass-Spectrom Ion Proc 59:125–142

Hanchar JM, Miller CF, Wooden JL, Bennett VC, Staude J-MG (1994) Evidence from xenoliths for a dynamic lower crust, eastern Mojave Desert, California. J Petrol 35:1377–1415

Heaman LM, Grotzinger JP (1992) 1.08 Ga diabase sills in the Pahrump Group, California: implications for the development of the Cordilleran miogeocline. Geology 20:637–640

Irvine TN, Baragar WRA (1971) A guide to the chemical composition of the common volcanic rocks. Can J Earth Sci 8:523–548

John BE, Wooden J (1990) Petrology and geochemistry of the metaluminous to peraluminous Chemehuevi Mountains Plutonic Suite, southeastern California. In: Anderson JL (ed) The nature and origin of Cordilleran magmatism. Geol Soc Am Mem 174:71–98

Karlstrom KE, Miller CF, Kingsbury JA, Wooden JL (1993) Pluton emplacement along an active ductile thrust zone, Piute Mountains, southeastern California: interaction between deformational and solidification processes. Geol Soc Am Bull 105:213–230

Kistler RW, Peterman ZE (1973) Variations in Sr, Rb, K, Na, and initial Sr87/Sr86 in Mesozoic granitic rocks and intruded wall rocks in Central California. Geol Soc Am Bull 84:3489–3512

Kistler RW, Peterman ZE (1978) Reconstruction of crustal blocks of California on the basis of initial strontium isotopic compositions of Mesozoic granitic rocks. US Geol Surv Prof Pap 1071

Kistler RW, Chappell BW, Peck DL, Bateman PC (1986) Isotopic variation in the Tuolumne Intrusive Suite, central Sierra Nevada, California. Contrib Mineral Petrol 94:205–220

Le Maitre RW (ed) (1989) A classification of igneous rocks and glossary of terms – recommendations of the International Union of Geological Sciences Subcommission on the Systematics of Igneous Rocks. Blackwell, Oxford

Mahood GA, Nibler GE, Halliday AN (1996) Zoning patterns and petrologic processes in peraluminous magma chambers: Hall Canyon pluton, Panamint Mountains, California. Geol Soc Am Bull 108:437–453

Martin MW, Walker JD (1992) Extending the western North American Proterozoic and Paleozoic continental crust through the Mojave Desert. Geology 20:753–756

McKenna LW, Sterns SM, Whitmarsh R, Baer E (1993) Pre-Late Jurassic extension and subsequent East Sierra thrusting in the

southern Cordillera of California. Geol Soc Am Abstr Program 25:A-284

Miller CF, Wooden JL (1994) Anatexis, hybridization and the modification of ancient crust: Mesozoic plutonism in the Old Woman Mountains area, California. Lithos 32:111–133

Miller CF, Wooden JL, Bennett VC, Wright JE, Solomon GC, Hurst RW (1990) Petrogenesis of the composite peraluminous-metaluminous Old Woman-Piute Range batholith, southeastern California; isotopic constraints. In: Anderson JL (ed) The nature and origin of Cordilleran magmatism. Geol Soc Am Mem 174:99–109

Miller JS, Glazner AF (1995) Jurassic plutonism and crustal evolution in the central Mojave Desert, California. Contrib Mineral Petrol 118:379–395

Miller JS, Glazner AF, Walker JD, Martin MW (1995) Geochronologic and isotopic evidence for Triassic–Jurassic emplacement of the eugeoclinal allochthon in the Mojave Desert region, California. Geol Soc Am Bull 107:1441–1457

Miyashiro A (1974) Volcanic rock series in island arcs and active continental margins. Am J Sci 274:324–355

Rämö OT, Calzia JP (1998) Nd isotopic composition of cratonic rocks in the southern Death Valley region: evidence for a substantial Archean source component in Mojavia. Geology 26:891–894

Richard P, Shimizu N, Allègre CJ (1976) $^{143}Nd/^{146}Nd$, a natural tracer: an application to oceanic basalts. Earth Planet Sci Lett 31:269–278

Sisson TW, Grove TL, Coleman DS (1996) Hornblende gabbro sill complex at Onion Valley, California, and a mixing origin for the Sierra Nevada batholith. Contrib Mineral Petrol 126:81–108

Stacey JS, Kramers JD (1975) Approximation of terrestrial lead isotope evolution by a two-stage model. Earth Planet Sci Lett 26:207–221

US Geological Survey (1991) Evaluation of metallic mineral resources and their geographic controls in the Eastern Mojave National Scenic Area, San Bernardino County, California. US Geol Surv Open-File Rep 91-427

Walker JD, Wardlaw, BR (1989) Implications of Paleozoic and Mesozoic rocks in the Soda Mountains, northeast Mojave Desert, California, for late Paleozoic and Mesozoic Cordilleran orogenesis. Geol Soc Am Bull 101:1574–1583

Wooden JL, Miller DM (1990) Chronologic and isotopic framework for Early Proterozoic crustal evolution in the eastern Mojave Desert region, SE California. J Geophys Res 95(B12):20133–20146

Wooden JL, Stacey JS, Howard KA (1988) Pb isotopic evidence for the formation of Proterozoic crust in the southwestern United States. In: Ernst WG (ed) Metamorphism and crustal evolution, western conterminous United States; Rubey vol 7. Prentice-Hall, Englewood Cliffs, pp 68–86

Wright LA (1967) Talc deposits of the southern Death Valley–Kingston Range region, California. Calif Div Mines Geol Spec Rep 95

Wrucke CT Jr (1966) Precambrian and Permian rocks in the vicinity of Warm Spring Canyon, Panamint Range, California. PhD Thesis, University of California, Stanford

Young ED, Wooden JL, Shieh Y-N, Farber D (1992) Geochemical evolution of Jurassic diorites from the Bristol Lake region, California, USA, and the role of assimilation. Contrib Mineral Petrol 110:68–86